



Aalborg Universitet

**AALBORG UNIVERSITY**  
DENMARK

## Inhomogeneity in Gass Forming Melts

Jensen, Martin

*Publication date:*  
2011

*Document Version*  
Publisher's PDF, also known as Version of record

[Link to publication from Aalborg University](#)

*Citation for published version (APA):*  
Jensen, M. (2011). *Inhomogeneity in Gass Forming Melts*. Faculty of Engineering and Science, Aalborg University.

### General rights

Copyright and moral rights for the publications made accessible in the public portal are retained by the authors and/or other copyright owners and it is a condition of accessing publications that users recognise and abide by the legal requirements associated with these rights.

- Users may download and print one copy of any publication from the public portal for the purpose of private study or research.
- You may not further distribute the material or use it for any profit-making activity or commercial gain
- You may freely distribute the URL identifying the publication in the public portal -

### Take down policy

If you believe that this document breaches copyright please contact us at [vbn@aub.aau.dk](mailto:vbn@aub.aau.dk) providing details, and we will remove access to the work immediately and investigate your claim.

# Aalborg University

## INHOMOGENEITY IN GLASS FORMING MELTS

Ph. D. Dissertation

by

Martin Jensen

Date of Defence

30.09.2011

Assessment committee:

Lena Hupa  
Associate Professor  
Åbo Akademi University, Finland

Russel J. Hand  
Dr., Reader  
The University of Sheffield, United Kingdom

Morten L. Christensen (Chairman)  
Associate Professor  
Aalborg University, Denmark

Supervisor:

Prof. Yuanzheng Yue  
Aalborg University, Denmark

## Preface

This dissertation is submitted to the Faculty of Engineering and Science at Aalborg University in the fulfilments of the requirements for obtaining the Ph. D. degree. The work is presented as a plurality and features an introduction to the topic and a discussion of key theoretical issues. It also contains a presentation of discussion of the key findings of the work. The results of the work are published in 7 papers.

The Ph. D. study was carried out at the Section of Chemistry at the Department of Biotechnology, Chemistry and Environmental Engineering at Aalborg University from September 2008 to August 2011. The project is an industrial collaboration project between Aalborg University and Rockwool International. Therefore, the project is partly funded by Rockwool International.

I would like to thank Long Zhang for providing me with the opportunity to perform parts of my research at his facilities at the Shanghai Institute of Optics and Fine Mechanics. In addition I would like to acknowledge the students S. Fjendbo, H. H. Poschwatta, B. H. Hede, H. Lundø, L. S. Trankjær, M. Jensen, R. E. Gissel and S. S. Damkjær who through their student project have contributed to the results of this work. K. Mørkholt and H. Koch are acknowledged for construction of the induction furnace used in the melting experiments. M. Solvang is acknowledged for many useful discussions throughout the project.

## Abstract

The presence of inhomogeneities such as bubbles and striae in glasses influences the physical and chemical performance of glass products. Due to the negative impact of inhomogeneities on glass products, glass scientists and technologists have for more than a century studied inhomogeneities and tried to eliminate them. Despite much progress in enhancing the homogeneity of glasses, scientists and technologists are still facing problems with quantification and elimination of inhomogeneities in glass products, and with clarification of the sources of the inhomogeneities. Part of the reason for those problems is a lack of reliable and universal methods for characterisation of the inhomogeneities. Another part of the reason is that the technological possibilities available to scientists and technologists decades ago are lower than those available today.

In the present Ph. D. project, methods for quantitative characterisation of bubbles and striae in glasses are developed. To characterise the striae, an optical image of the investigated glass is acquired and subjected to image analysis. The presence of a stria influences the optical transmission of the glass in the striated domain and therefore, the striae in the glass are identified by changes in the optical transmission of the sample. The optical transmission is recorded along a line on the acquired image, which is referred to as line scanning. For each glass sample, 500 line scans undergo Fourier transformation in order to obtain the stria intensity as a function of stria dimension. The stria intensity is a measure of the optical transmission difference between the striae and the glass matrix. The striae in the glass are characterised by a characteristic dimension and intensity or the total stria content of the glass. The bubble content in glass samples is determined by acquisition of 2D images stacks by means of optical microscopy. A computer program identifies the bubbles on the acquired image stacks and determines the volume of each bubble.

The stria content in a glass melt is reduced by stirring the melt, increasing the melt temperature, and prolonging the retention time. Striae are equilibrated by diffusion. Increasing melt temperature enhances the diffusion rate, and hence, reduces the stria content in the resulting glass. A prolonged retention time increases the extent of diffusion and thereby diminishes the stria content of the melt. Stirring in itself does not eliminate striae from the melt, but stirring reduces the dimension of the striae in the melt. The smaller dimension of the striae allows a faster elimination of them. In an iron-bearing calciumaluminosilicate melt (melt used for stone wool production) both striae caused by gradients in the chemical composition and striae caused by a change in the  $\text{Fe}^{2+}/\text{Fe}^{3+}$  ratio have been identified. In the stone wool melt, an increase in the melt temperature causes a growth of the bubbles, whereas the overall bubble volume is unaffected by the temperature increase. Bubbles with a diameter smaller than 25  $\mu\text{m}$  are mostly filled with  $\text{CH}_4$ ,  $\text{CO}$  and  $\text{CO}_2$ , whereas the bubbles larger than 25  $\mu\text{m}$  mainly contain  $\text{N}_2$ ,  $\text{H}_2\text{S}$  and  $\text{SO}_2$ .

## Dansk resume (Danish abstract)

Tilstedeværelsen af uhomogeniteter som bobler og slirer i glas har indflydelse på glasproduktets egenskaber. På grund af uhomogeniteternes negative indflydelse på glasegenskaberne, er uhomogeniteterne og deres eliminering blevet studeret gennem århundreder. På trods af betydelige fremskridt i den generelle glashomogenitet gennem de sidste hundrede år forårsager kvantificeringen og elimineringen af uhomogeniteter stadig problemer ligesom en fastlæggelse af uhomogeniteternes oprindelse er vanskelig. En del af forklaringen på de problemer der er med uhomogeniteter i glasprodukter skyldes en mangel på pålidelige og universelle metoder til karakterisering af uhomogeniteter i glas. En andel del af forklaringen er at forskere tidligere ikke har haft adgang til de samme teknologiske muligheder som er tilgængelige for nutidens forskere.

I dette Ph. D. projekt udvikles metoder til kvantitativ beskrivelse af bobler og slirer i glasser. Slirerne undersøges ved at tage et billede af glasprøven og anvende dette til en billedanalyse. Slirer i glasser bevirker en ændring af den optiske transmission i det slirede område og derfor karakteriseres slirerne ud fra ændringerne i glassens optiske transmission. Glassens optiske transmission måles langs en linje på billedet, hvilket benævnes linjeskanning. For hver prøve udføres 500 linjeskanninger der hver udsættes for Fourier transformation for at bestemme slireintensiteten som funktion af sliredimensionen. Slireintensiteten er et mål for forskellen i optisk transmission mellem sliren og den omkringliggende homogene glas. Slirerne i en glas er kvantificeret ud fra en karakteristisk dimension og intensitet eller glassens totale slireindhold. Bobleindholdet i glasprøver bestemmes ved at fremstille en stak af 2D billeder ved hjælp af optisk mikroskopi. Et computerprogram identificerer boblerne i billedstakken og bestemmer voluminet af hver enkelt boble.

Slireindholdet i en glassmelte reduceres ved omrøring, øget smeltetemperatur og forlænget smeltetid. Slirer i glassmelten udlignes via diffusion. Højere smeltetemperatur øger diffusionshastigheden og reducerer derved slireindholdet i smelten. En længere smeltetid øger diffusionsomfanget og reducerer på denne måde smeltens slireindhold. Omrøring i sig selv eliminerer ikke slirer fra glassmelten, men omrøring mindsker slirernes dimensioner i smelten. De mindre sliredimensioner fører til en hurtigere eliminering af slirerne via diffusion. I en jernholdig calciumaluminiumsilikat smelte (smelte anvendt i produktion af stenudd) findes slirer der skyldes en gradient i den kemiske sammensætning samt slirer som skyldes en forskel i  $\text{Fe}^{2+}/\text{Fe}^{3+}$  niveauet. I en industrielt produceret stenuddsmelte forårsager en forøget smeltetemperatur større bobler, omend det samlede boblevolumen forbliver uændret. Bobler med en diameter mindre end 25  $\mu\text{m}$  indeholder hovedsageligt  $\text{CH}_4$ ,  $\text{CO}$  og  $\text{CO}_2$  mens bobler større end 25  $\mu\text{m}$  mest består af  $\text{N}_2$ ,  $\text{H}_2\text{S}$  og  $\text{SO}_2$ .

## Table of contents

1	Introduction.....	1
1.1	Motivation.....	1
1.2	Scope of the thesis .....	1
1.3	Outline of the thesis .....	2
2	Background.....	3
2.1	Glass production .....	3
2.2	Origin of inhomogeneities in glass .....	4
2.2.1	Bubbles .....	5
2.2.2	Undissolved raw materials (stones) .....	5
2.2.3	Striae .....	6
2.2.4	Recrystallized species .....	6
2.3	Methods for characterisation of glass homogeneity .....	7
2.3.1	Christiansen filter method .....	7
2.3.2	Measurement of chemical composition .....	9
2.3.3	Refractive index measurement.....	9
2.4	Establishment of a stria characterisation method .....	10
2.4.1	Transmission of light through glass .....	10
2.4.2	Processing of transmission data.....	13
2.5	Characterisation of bubbles .....	13
3	Characterisation of striae and bubbles.....	15
3.1	Characterisation of striae.....	15
3.1.1	Image acquisition .....	15
3.1.2	Image processing .....	16
3.1.3	Line scanning.....	17
3.1.4	Fourier transformation .....	18
3.2	Quantification of bubble size.....	18
3.2.1	Image stack acquisition .....	18
3.2.2	Image processing .....	18
3.2.3	Image analysis .....	19
4	Characterisation of inhomogeneities.....	20
4.1	Stria characterisation.....	20
4.1.1	Characterisation of simulated striations .....	20
4.1.2	Characterisation of glasses from stone wool melts .....	22
4.1.3	Discussion of the stria characterisation method .....	24
4.2	Ranking the homogeneity of glass .....	26
4.3	The chemical origin of the striae .....	29
4.3.1	Method verification .....	30
4.3.2	Characterisation of glasses from stone wool melts .....	31
4.4	Bubble characterisation .....	33
4.4.1	Bubble size distribution .....	33
4.4.2	Chemical analysis of gaseous species.....	34

---

5	Influence of production conditions on inhomogeneities.....	36
5.1	Equilibration of striae in glass melts.....	36
5.1.1	Effect of stirring on striae in glass melts: Simulation studies .....	36
5.1.2	Effect of stirring on striae in glass melts: Experiments .....	38
5.1.3	Effect of melting temperature and retention time on stria equilibration .....	39
5.1.4	Effect of melt viscosity on stria equilibration.....	42
5.2	Removal of bubbles from glass melts .....	43
5.2.1	Influence of melt temperature on bubble content .....	44
5.2.2	Influence of iron on bubble content.....	45
6	Summary .....	47
7	Bibliography .....	49

Paper 1: Quantification of chemical striae in inorganic melts and glasses through picture processing. *Journal of the American Ceramic Society* 93 (2010) 2705-2712.

Authors: M. Jensen, R. Keding & Y. Z. Yue

Paper 2: Effect of bubbles on the characterisation of striae. *Glass Technology: European Journal of Glass Science and Technology Part A* 51 (2010) 147-152.

Authors: M. Jensen, R. Keding, S. Fjendbo, H. H. Poschwatta & Y. Z. Yue

Paper 3: Homogeneity of inorganic glasses: Quantification and ranking. *International Journal of Applied Glass Science* 2 (2011) 137-143.

Authors: M. Jensen, L. Zhang, R. Keding & Y. Z. Yue

Paper 4: Probing iron redox state in multicomponent glasses by XPS. *Chemical Geology*, submitted.

Authors: M. Jensen, L. Zhang & Y. Z. Yue

Paper 5: Bubble formation in basalt-like melts. *Glass Technology: European Journal of Glass Science and Technology Part A* 52 (2011) 127-135.

Authors: M. Jensen, R. Keding & Y. Z. Yue

Paper 6: Effect of stirring on striae in glass melts. *Journal of Non-Crystalline Solids*, under review.

Authors: M. Jensen & Y. Z. Yue

Paper 7: Effect of melting conditions on striae in iron-bearing silicate melts. *Glass Technology: European Journal of Glass Science and Technology Part A*, submitted.

Authors: M. Jensen & Y. Z. Yue

# 1 Introduction

## 1.1 Motivation

Glass is a material that through the past centuries has found increased use and is now applied in many modern technologies and daily uses such as containers, telescopes, optical communication fibres, windows, insulation materials, lenses, display panels, solar cell panels, composite materials and buildings. Depending on the application fields, glass is produced by different means and from different raw materials. Despite this diversity, the vast majority of glasses are produced through a procedure with the following common features. Since a given glass is produced from a batch of raw materials each with a different chemical composition, the raw materials need to be mixed initially. The mixed batch is then loaded into a melting furnace where the raw materials melt upon heating. During the melting process, the differences in chemical composition between each of the raw materials are gradually homogenised through diffusion. Besides inflicting a melting of the raw materials, the heating of the raw materials can lead to generation of bubbles. Owing to buoyancy, the bubbles rise to the surface, however, if the melting temperature is too low or the melting duration is too short, the bubbles are entrapped in the melt. A bubble-free melt where all raw materials have been melted and the chemical differences of the raw materials have been equilibrated is said to be homogeneous, whereas an inhomogeneous melt contains bubbles and/or differences in the chemical composition or even undissolved raw materials. Any inhomogeneity present in the melt is transferred to the final glass product, which leads to a deterioration of the performance of the product [Abrams & Green 2006; Beerkens & van der Schaaf 2006; Lund & Yue 2008; Svecova et al 2010]. Therefore, control of the homogeneity of glass melts is a key issue for both glass industry and glass research.

Due to the importance of homogeneity of glass, researchers have been trying to characterise and study it and to find different approaches to enhance it for centuries [Christiansen 1884; Tooley & Tiede 1946; Shelyubskii 1960; Varshneya et al 1985; LaTourette et al 1995; Hoffmann, 2003]. The characterisation and evaluation of glass homogeneity have been performed by means of various methods, e.g. based on optical measurements [Braetsch & Frischat 1988; De Freitas & Player 1995; Hoffmann 2000], compositional measurements [Behrens & Haack, 2007; Wondraczek et al 2007; Chopinet et al 2010] and other kinds of measurements [Jerie et al 1999; Souza et al 2005]. These methods are useful in one or another case, but are not universal, and in some situations they are complicated and inaccurate. This is often due to low sensitivity of those methods to compositional fluctuations and redox changes and to complexity of the measurements (time consuming measurements). Thus, a universal and simple method for characterising the homogeneity of glasses needs to be established.

Development of one or several methods for characterisation of glass homogeneity does not in itself lead to homogeneous glass products. Accurate homogeneity characterisation is a requisite for exploration of the effect of melting conditions on the homogeneity of the final glass product, and for finding the sources of its inhomogeneity.

## 1.2 Scope of the thesis

Studies of homogeneity can take place from the atomic scale to the macroscopic scale. In this work, focus is on macroscopic inhomogeneities, i.e., inhomogeneities in the size range  $\mu\text{m}$  to  $\text{cm}$ . In this size range, homogeneity is controlled by several aspects such as striae, bubbles, crystals and undissolved raw materials.

Therefore, the work needs to be limited to focus on some of these factors. This work is devoted to the two most common inhomogeneities in glasses: striae and bubbles. Therefore, the aims of the project are as follows:

1. Develop methods for characterisation of striae and bubbles in glasses
2. Find characteristic quantities for describing homogeneity of glass
3. Perform a universal ranking of glasses based on their homogeneity
4. Explore the chemical origin of the striae in the investigated glasses
5. Clarify the effect of production conditions on the homogeneity of glass

## **1.3 Outline of the thesis**

The thesis is presented as a plurality including an introductory overview followed by 7 papers based on the research from the project (4 published and 3 submitted). The overview provides the background and key analysis methods employed in the project. The papers are:

1. Quantification of chemical striae in inorganic melts and glasses through picture processing
2. Effect of bubbles on the characterisation of striae in glasses
3. Homogeneity of inorganic glasses: Quantification and ranking
4. Probing iron redox state in multicomponent glasses by XPS
5. Bubble formation in basalt-like melts
6. Effect of stirring on striae in glass melts
7. Effect of melting conditions on striae in iron-bearing silicate melts

## 2 Background

From a physical perspective, a glass is a substance without a long range order, i.e., the substance only contains domains with ordered structures smaller than  $\sim 10$  nm. From this definition, the term “glassy” can be used to describe a broad range of materials such as window glass, metals, chalcogenides and organic polymers, etc. In the present work, description of the background of inhomogeneities solely deals with oxide glasses, i.e., the glass contains oxygen anions and different cations.

The project is performed in the frame of collaboration between Rockwool International A/S and Aalborg University. The Rockwool group is the world’s leading supplier of products and systems of stone wool. The production of stone wool insulation fibres differs from that of ordinary inorganic oxide glass products such as container glass in some aspects. The general production steps of both stone wool fibres and common oxide glass are discussed. The origin of inhomogeneities in glasses in general is discussed. In the present work, samples from both stone wool melts, common oxide glasses, and glasses produced at laboratory scale will be studied with respect to inhomogeneities.

### 2.1 Glass production

The main difference between common oxide glass production and the production of stone wool is the redox conditions of the melt during the melting process. Oxide glasses are commonly produced under neutral or oxidising conditions, whereas stone wool is produced under reducing conditions. A similarity between these glass production processes is heating of the raw material batch to the molten state. After a certain retention time in the furnace, the melt is cooled at a high rate. For stone wool, the cooling rate of the melt is as high as  $10^6$  K/s during the fibre spinning process [Yue et al 2004]. If a low cooling rate is applied, crystals can form when the temperature is below the melting temperature since the crystalline structure possesses a lower energy state than the glass structure. To circumvent crystal formation, a high cooling rate is applied, which shortens the time window for atomic rearrangement into the ordered crystalline structure. Instead of crystallising, a disordered glass structure is obtained when the melt is cooled to such an extent where a high viscosity prevents further atomic movement. This point is at a viscosity of  $10^{12}$  Pa s, which is also known as the glass transition temperature ( $T_g$ ) [Yue 2008].

The melting procedure of common oxide glass production can be described by considering the setup used for the production of the highly prevalent container glass. Container glass is produced in a tank furnace that is divided into two chambers: the melting chamber and the working chamber. The raw materials are loaded into the melting chamber where the raw materials melt upon heating. The melt is in contact with an air atmosphere above the melt. Bubbles entrapped in the melt ascend to the surface due to buoyancy unless the ascent is kinetically hindered by a high viscosity. After a certain retention time in the melting chamber, the melt flows into the working chamber where the temperature is lower than in the melting chamber. In the working chamber, remaining gradients in the chemical composition of the melt can be equilibrated and the melt obtains the desired viscosity for the forming process. The furnace is commonly fired by burning fossil fuels such as gas or coal outside the furnace followed by a direction of the flame from the combustion process into the furnace. Since the melt is not in contact with the fuel and there is atmospheric air above the melt in the furnace, the conditions in the container glass furnace are oxidising [Persson, 1983].

Stone wool melts belong to the iron-bearing calciumaluminosilicate system. Most stone wool melts are produced by loading lumps of raw materials and coke into the top of a cupola furnace [Leth-Miller et al

2003]. Nozzles used for adding pre-heated air to the furnace are placed at the bottom of the furnace (Figure 2.1).

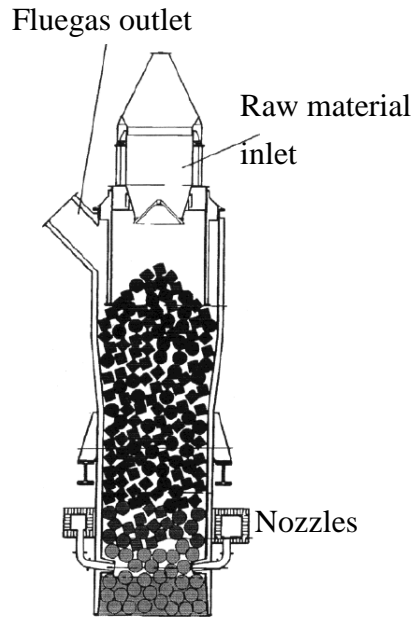


**Figure 2.1:** Illustration of a cupola furnace used in stone wool production modified from [Leth-Miller et al 2003]. Pre-heated atmospheric air is supplied to the furnace at the nozzles.

Through reaction with oxygen in the blown-in air, coke combusts and thereby acts as energy source for the furnace [Širok et al 2008]. Besides reacting with molecular oxygen, coke can undergo oxidation by reaction with iron oxides in the raw materials and this reaction is responsible for creating the reducing conditions inside the furnace [Leth-Miller et al 2003]. Besides cupola furnaces, electric furnaces are also used in production of stone wool melts. In the electric furnace, graphite electrodes directly heat the stone wool melt. In both the electric and cupola furnace lumps of raw materials are loaded into furnace, but the retention time (duration between raw materials are loaded into the furnace and the melt leaves the furnace) is 10 to 20 times longer in the electric furnace than in the cupola furnace. Both the cupola and the electric furnace operate around a temperature of 1500 °C and under reducing conditions. Melt has also been sampled from a test furnace where finely ground raw materials are used, but due to confidentiality no details about the operating conditions can be provided for this furnace.

## 2.2 Origin of inhomogeneities in glass

Inhomogeneities in glass are closely related to the glass production procedure. The composition of a glass product is tailored from the desired properties of the product. To obtain the desired glass properties, it is necessary to produce a batch from several chemically different raw materials. After the batch is mixed, it is melted at an elevated temperature at which the melt fining and homogenisation processes occur. The melting temperature depends on the batch composition. If the fining process is incomplete, bubbles appear and remain in the melt (Figure 2.2). The well fined and homogenised melt is free of bubbles and has a uniform chemical composition. Each of the most common inhomogeneities in glasses and their origin is discussed in subsection 2.2.1 through 2.2.4.

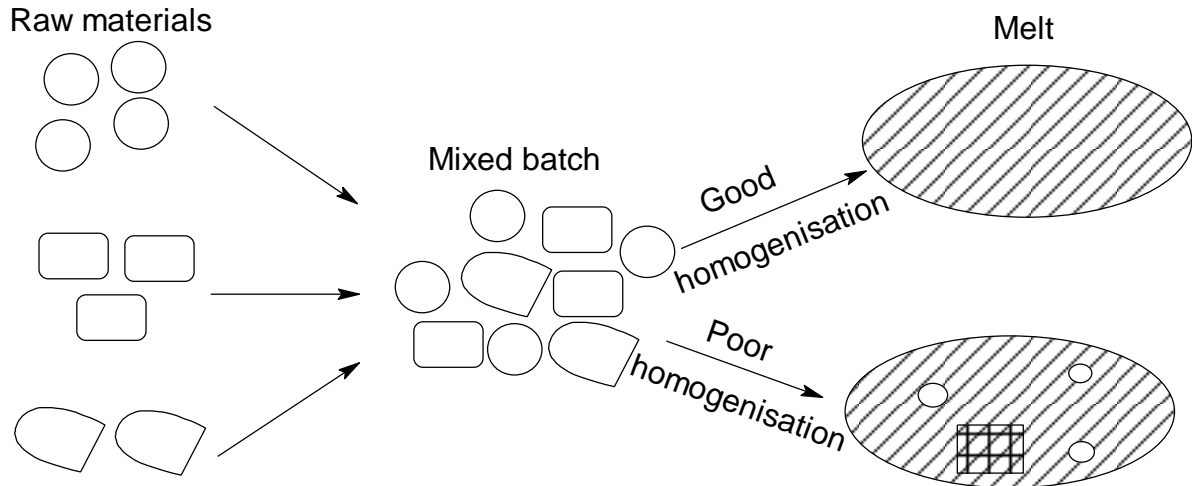


**Figure 2.2:** Mixing of raw materials and the homogenisation that occurs during melting of the raw materials. In the poorly homogenised melt bubbles and a domain with a different chemical composition (differently hatched area) and three bubbles (white areas) are found

### 2.2.1 Bubbles

The occurrence of bubbles can have several possible origins. First, in the mixed batch, voids between the raw materials are present (Figure 2.2). Due to the difference in chemical composition between the various raw materials, the melting temperature between raw materials differs. When the raw material with the lowest melting temperature melts, it flows and covers the other still solid raw materials. The consequence is an encapsulation of the voids between the raw materials in the initial batch and thereby these voids become gaseous inclusions in the freshly obtained melt. Another possibility for encapsulation of voids is sintering of raw materials before the melting, which also causes an encapsulation of the air in the gaps between the raw materials. Second, commonly, some of the raw materials used in glass production are present as carbonates, which upon heating decompose to oxide and  $\text{CO}_2$ . Third, any moisture in the raw materials is released as water vapour upon heating. Fourth, the glass melt can dissolve the refractory stones that constitute the wall of the furnace. For porous refractory stones, the air in the pores is released and then entrapped in the melt [Mulfinger, 1980]. Fifth, bubble generation sources specific for a certain melting technology can exist. Such an example is the cupola furnace which is fired by combusting coke inside the furnace. Since coke is in direct contact with the raw materials during the combustion process, reactions between coke and species in the raw materials or melt could take place. An example of this is the reduction of  $\text{Fe}_2\text{O}_3$  to  $\text{FeO}$  or the reduction of  $\text{FeO}$  to  $\text{Fe}^0$  by means of coke [Leth-Miller et al 2003]. During the reduction of both  $\text{Fe}_2\text{O}_3$  and  $\text{FeO}$ , coke is oxidised to  $\text{CO}$  and/or  $\text{CO}_2$  depending on the local redox conditions.

### 2.2.2 Undissolved raw materials (stones)

As stated in subsection 2.2.1, the melting temperature of the raw materials in a batch differs. During the melting process, the raw materials with the lowest melting point initially form a melt in which the raw materials with the higher melting temperature reside. The stones gradually dissolve in the surrounding melt as the temperature increases. Since the dissolution of the raw materials depends on both the melting temperature and the duration at the melting temperature, a low melting temperature and short retention time can cause incomplete dissolution of all raw materials. In that case, small grains of undissolved raw materials are present in the melt as it leaves the furnace.

### 2.2.3 Striae

A stria is a domain within the glass that differs chemically and/or physically from the surrounding glass matrix. Hence, a stria can be described as “glass in glass”. Striae can be divided into chemical and physical ones. In the former, both the chemical and physical properties differ from the surrounding glass whereas the latter only displays a difference in the physical properties compared to the parent glass [Brückner 1980].

The physical stria arises when the cooling rate of the melt during the casting process is inhomogeneous. Since the energy state and volume of the glass depend on the cooling rate [Shelby 2005], a fluctuation in these two parameters exists in a glass sample with a cooling rate gradient. As a consequence, a difference in packing density between the stria and the glass is present, which among others leads to a fluctuation in the refractive index across the physically striated region.

The chemical stria has two potential origins. It can be a fluctuation in the chemical composition or it can be a change in redox state if the glass contains polyvalent elements. The difference in chemical composition has several potential sources. First, the compositional difference between the raw materials in the batch is equilibrated by the entropy driven diffusion process when the raw materials have entered the molten state. The diffusion rate of ions in the glass melt depends on the temperature of the melt [Schoo & Mehrer 2000; Grofmeier et al 2007; Smedskjaer et al 2010]. Hence, similar to the dissolution of raw materials described in subsection 2.2.2, a low melting temperature and a short melting duration can be insufficient to equilibrate the differences in chemical composition that exist immediately after the last raw materials have been dissolved in the melt. Depending on the extent of diffusion during the melting process, the extent of the chemical differences in the stria can vary. Due to the complexity of chemical striations, a chemical stria can be caused by a fluctuation in a single or several species. Consequently, each chemical stria affects the chemical and physical properties to different extents. A chemically striated glass can contain striae with fluctuations in different chemical species, which even can possess various concentration gradients across different domains of the glass. Second, alkalis can evaporate from the melt during the melting process and consequently the surface of the glass melt is depleted in alkali ions. Third, the inside of the glass furnace tank is made by a refractory material and during the melting process parts of the refractories can dissolve in the glass melt [Brückner 1980].

The other type of chemical striae, the striae created by a variation in the redox state, can have two possible origins. First, local redox conditions might exist in the melt and therefore, domains with a different oxidation state can occur in the glass melt. Second, after the melt leaves the furnace, it might be exposed to both a different atmosphere (redox conditions) and a sudden temperature change. The temperature of the melt affects the equilibrium oxidation state of polyvalent elements in the melt since the redox state shifts towards a more oxidised state when the temperature is decreased [Dingwell & Brearley 1988; Lange & Carmichael 1989; Kukkupadu *et al* 2003; Kaufmann & Rüssel 2010]. During the melting procedure in the cupola furnace, some parts of the melt are in direct contact with coke, whereas others parts of the melt are less exposed to the reducing conditions of the coke, i.e., local variations in the redox state of the melt can exist.

### 2.2.4 Recrystallized species

Crystalline domains in a glass can be both undissolved raw materials and re-formed crystals. Whereas the undissolved raw materials in the glass are present due to an insufficient melting process (subsection 2.2.2), the re-formed crystals are created after the melt has left the furnace, i.e., during the glass forming process. Since the energy of the crystalline state is lower than that of the glassy one, there is a thermodynamic driving

for the crystal formation when the melt is cooled. In glass production, the crystallisation is avoided by rapidly quenching the melt. Due to the high cooling rate, the available time for atoms to rearrange into the ordered structure is insufficient and instead the disorder of the atoms in the melt is frozen in, i.e., the glass state forms. The cooling rate which is necessary to avoid crystal formation varies by orders of magnitudes between different glass compositions [Shelby, 2005]. Theoretically, crystals can form in any liquids as long as the cooling process is slow enough.

## 2.3 Methods for characterisation of glass homogeneity

As explained in section 2.2, inhomogeneities are very different in their chemical and physical nature and originate from different sources. Due to this complexity, several methods have been established to characterise the homogeneity of glasses. Some of the methods are sensitive to few of the types of inhomogeneities whereas others only concern a single type of inhomogeneity. In this section some of the key approaches for homogeneity characterisation are presented and discussed.

### 2.3.1 Christiansen filter method

The Christiansen filter method is based on measurement of the transmission of optical light developed by Christiansen more than a century ago [Christiansen 1884; Christiansen 1885]. The filter contains irregularly shaped glass grains immersed in a fluid with a refractive index close to that of the glass (Figure 2.3).

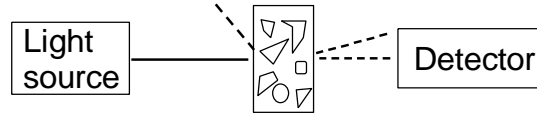


**Figure 2.3:** Schematic illustration of a Christiansen filter. A monochromatic light source (typically a laser), irradiates the irregularly shaped glass grains immersed in a fluid which leads to absorbed, reflected, refracted and transmitted light (dashed lines).

During the operation of the Christiansen filter setup, the transmittance of light through the filter is recorded as a function of either wavelength of the incident light or the temperature of the filter. The method relies on the different refractive index dependence on wavelength and temperature for the glass and the immersion fluid (Figure 2.4).

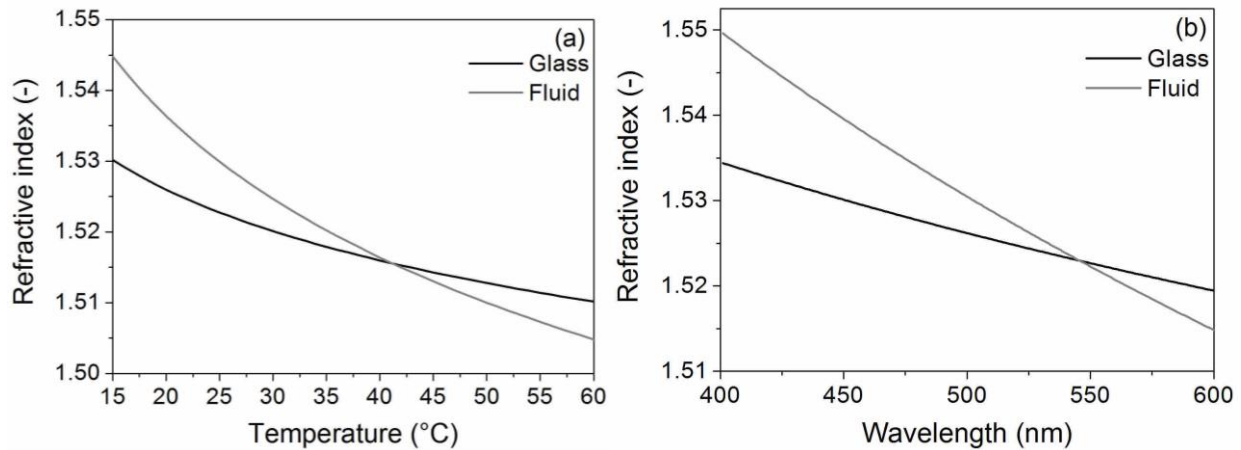


**Figure 2.4:** Dependence of refractive index of the glass grains and immersion liquid on temperature at a fixed wavelength (a) and wavelength of the incident light at a fixed temperature (b).

The refractive indices of the fluid and the glass match at a given temperature or given wavelength. At the intersection point of the two curves, reflection and refraction of the incident light reaches a minimum, i.e.,

the transmission of the filter is maximised. The refractive index curves of the glass grains correspond to a certain chemical composition, i.e., to a homogeneous glass. Each chemical domain in the glass exhibits its own refractive index behaviour. Therefore, in a situation where glass grains originating from an inhomogeneous glass are used in the filter, the filter contains glass grains with different refractive indices at a given temperature and grains with different dependencies of refractive index on temperature (Figure 2.5).

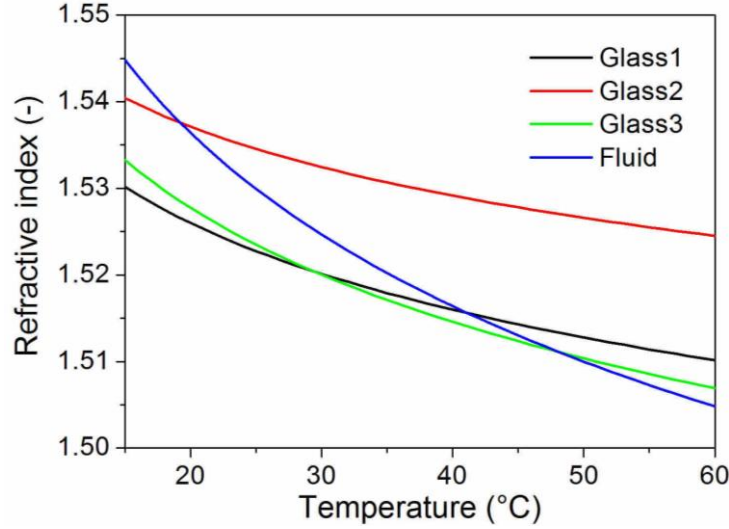


**Figure 2.5:** Refractive index against temperature for a filter with glass grains from a chemically inhomogeneous glass.

When the filter is filled with inhomogeneous glass, the match of the refractive index between the glass grain and immersion fluid occurs at various temperatures. Consequently, an increased optical transmission through the filter is seen at various temperatures, e.g., at 19, 41 and 48 °C as given in the example in Figure 2.5. In real samples, however, the refractive index match is likely to occur around a single temperature and the transmittance decays in a Gaussian manner from this temperature [Hoffmann 1999].

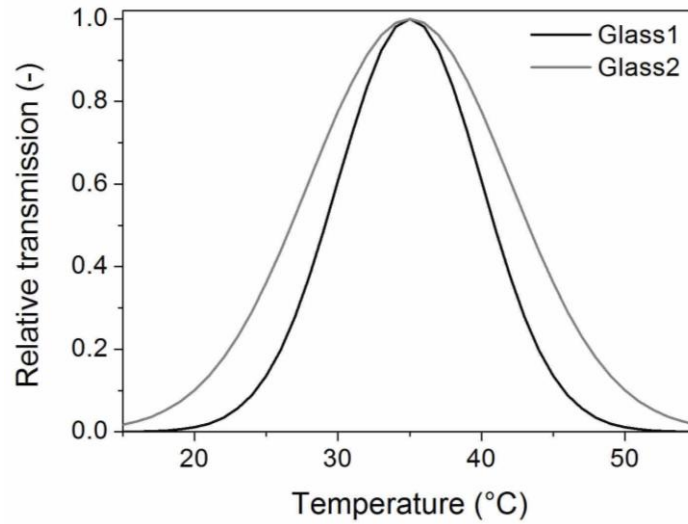


**Figure 2.6:** Relative transmittance through the Christiansen filter at different temperatures for a relatively homogeneous glass (Glass1) and a relatively inhomogeneous glass (Glass2). The maximum transmittance for each glass has been made relative to 1.

In Figure 2.6, the optical transmission as a function of temperature is shown for a relatively homogeneous glass (Glass1) and a relatively inhomogeneous glass (Glass2). The more inhomogeneous glass has a broader peak than the more homogeneous glass, since the inhomogeneous glass has refractive index match at several temperatures (cf. Figure 2.5). Comparison of transmission as a function of temperature does, however, only provide a qualitative description of the homogeneity of the glass. Based on the ideas of Raman [Raman

1949], Shelyubskii has established an approach for characterisation of the refractive index homogeneity of glass by means of Christiansen filter measurements [Shelyubskii 1960]. From the method of Shelyubskii, the peak width of the transmission curve at half transmission maximum can be used to determine the standard deviation of the refractive index in the glass. The formulae of Shelyubskii have intensively been applied to determine the homogeneity of glasses by means of Christiansen filters [Schilling & Weiss 1966; Inoue et al 1984; Varshneya 1986; Braetsch & Frischat 1988; Balasubramanian et al 1992; Tenzler & Frischat 1995; Janke & Frischat 1998]. Although critical comments from some authors [Afghan & Cable 1980; Varshneya et al 1985; Aylward et al 1986], the fact that the ideas of Raman (and consequently the extension by Shelyubskii) are inadequate and to some extent fundamentally wrong has been ignored. As noted in Hoffmann (2003), Raman assumed homogeneously distributed cubic grains, whereas irregularly shaped grains are randomly dispersed in the Christiansen filter. Also Raman's and Shelyubskii's formula states that the transmission of one grain with a certain diameter is smaller than the transmission through two grains with half the diameter, although the opposite phenomenon is valid [Hoffmann 2003]. Furthermore, the thoughts of Raman did not include contributions from Raleigh scattering, scattering between the glass, the immersion liquid and the wall of the filter (Fresnel reflection) and change in the aperture angles due to refraction [Hoffmann 1999]. In addition to these general issues, there are sample specific deficiencies. First, optically transparent glass grains are required, i.e., strongly light absorbing glasses such as iron-bearing glasses must be crushed to small pieces in order to obtain a transparent grain. As a consequence of the small grain size, only refractive index changes that occur over small dimensions can be detected. Second, the method cannot characterise absorption striae, i.e., the method is unable to describe changes in redox state of any polyvalent elements in the glass.

### **2.3.2 Measurement of chemical composition**

Measurement of the chemical composition in different domains of the glass directly addresses the chemical nature of the striations in contrast to the optical based approach applied in the Christiansen filter method. Previously, local measurements of chemical composition have mainly been carried out by the means of laser ablation inductively coupled plasma mass spectroscopy (LA-ICP-MS) [Schmidt et al 2004; Trejos & Almirall 2005; Sylvester 2006; Huang et al 2007; Nehring et al 2008] or electron microprobe measurements [LaTourette et al 1995; Canil 1999; Rocholl 1999; Pertermann & Hirschmann 2003; Behrens & Haack 2007; Vetere et al 2007; Chopinet et al 2010]. Since the equipment for direct measurement of chemical composition is more delicate and advanced than that used in, e.g., the Christiansen filter method, direct measurement of local chemical compositions dates only a few decades back. Many of the techniques used for measurement of chemical composition are insensitive to changes in redox state of polyvalent elements, however, more recent X-ray techniques such as X-ray absorption near-edge structure (XANES) and X-ray photoelectron spectroscopy (XPS) can determine the redox state of the species [Wilke et al 2005; Villian et al 2007; Backnaes et al 2008].

### **2.3.3 Refractive index measurement**

The refractive index across of a glass is normally measured by means of an interferometer [Puryayev 1998]. Besides being applied in refractive index quantification, interferometers can be used for qualitative description of striations [Kerkhof 1980]. From refractive index measurements of different spots on the glass, a standard deviation of the refractive index can be determined, i.e., a result similar to that of the Christiansen

filter method is obtained. However, data from interferometers are more reliable since there are fewer effects to be accounted for. A standard equipment is sensitive to refractive index variations of about  $5 \cdot 10^{-7}$  [Puryayev 1998], but with a more complex setup and very precise temperature control, sensitivities down to  $10^{-8}$  can be obtained [De Freitas & Player 1995]. Due to the nature of the interferometer, only refractive index induced striations can be measured, i.e., the method is insensitive to striae caused by changes in absorption due to different redox states of polyvalent elements.

## 2.4 Establishment of a stria characterisation method

Some glasses containing polyvalent elements such as iron could contain striae that arise from differences in the absorption of the glass. For such glasses, both the Christiansen filter method and the refractive index measurements are incapable of describing all striations. X-ray techniques such as XANES can detect changes in the redox state, but the measurements are time consuming. As a consequence of the slow data acquisition, the number of measurements has to be limited, and this increases the statistical uncertainty of such measurements. Especially for inhomogeneous glasses, the statistical aspect is crucial for clarifying whether a certain fluctuation of chemical composition is due to accidental presence of a lonely standing domain with different composition from the surrounding or is a more general feature throughout the whole sample. Therefore, it is necessary to develop a method which is sensitive to striae caused by changes in both refractive index and absorption of the glass and has fast data acquisition to reduce statistical uncertainty.

Measurement of the optical transmission of light through a sample is sensitive to striae caused both by refractive index changes and by changes in the absorption. To achieve a fast data acquisition rate, it is chosen to obtain an image of the glass. Instead of recording the transmission of the glass from the apparatus, the transmission of the entire image can be recorded by a computer at a fast rate. In other words, by analysing an image of the sample recorded by means of optical transmission, the requirements for a general and reliable stria characterisation method could be obtained. The disadvantage of optical transmission based approaches is that the chemical nature of the striations remains hidden.

Large amounts of transmission data are, however, insufficient to characterise striae since precise and quantitative description of striae require a solid and physically meaningful processing of the data. In order to establish such processing procedure, it is necessary to consider the chemical nature of the striae. The chemical striae arise since the dissolution of certain raw materials in the glass melt is incomplete. The chemical components of that raw material diffuse into the surrounding melt and create a gradient in the chemical species of that raw material around that particle. The gradient gradually diminishes from the particle/melt interface towards the homogenised glass melt. Therefore, chemical striae are soft oscillating changes in the chemical composition of one or more components. Consequently, the transmission changes caused by the striae could be mimicked by Fourier transformation, which fits sine curves to a data set. In the following subsections, the theoretical background behind the new stria characterisation method is presented. The details of the method are presented in Chapter 3.

### 2.4.1 Transmission of light through glass

Transmission is the ability of a material to permit light. When the incident light encounters the material four phenomena can occur: refraction, reflection, absorption and transmission. The extent of reflection and refraction is determined by the refractive index of the glass, i.e., the light velocity in the glass. For a chemically and physically homogeneous glass, each of the four parameters is constant for the entire glass. If the glass, how-

ever, contains inhomogeneities such as striae and bubbles, local fluctuations in the four phenomena are observed. In the following subsections each of the four parameters is described.

### Refraction

When light passes a domain with a refractive index different from that of the surrounding glass matrix, a displacement of the light occurs. The displacement ( $d$ ) over the distance  $l$  is determined by Eq. (2.1)

$$d = \Delta n \cdot l \quad (2.1)$$

Where  $\Delta n$  is the refractive index difference between the domain in question and the surrounding glass matrix. From Eq. (2.1) it is seen that the displacement of the light depends on both the refractive index difference (the striae intensity) and the sample thickness.

### Reflection

Reflection describes the phenomenon when light returns to the medium from which it originated instead crossing the interface to the new medium. Reflection is related to the refractive index of the glass by Snell's law, Eq. (2.2).

$$\frac{\sin \theta_1}{\sin \theta_2} = \frac{n_2}{n_1} \quad (2.2)$$

Where  $n_1$  and  $n_2$  are the refractive indices of medium 1 and 2, respectively and  $\theta_1$  and  $\theta_2$  are the angles of the ingoing and outgoing light, respectively. The path of light going from air to glass is illustrated in Figure 2.7.

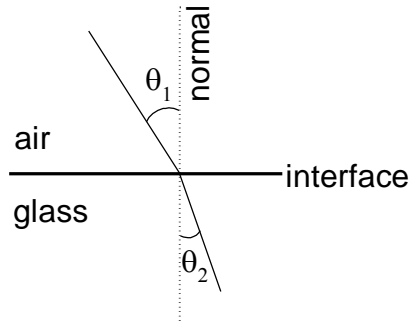


**Figure 2.7:** Illustration of the refraction of light that occurs when the light travels from air to glass.

After travelling through the glass, the light encounters the glass/air interface. If the glass is homogeneous, it is seen from Eq. (2.2) that the angle of the outgoing light is similar to that of the ingoing light at the air/glass interface. Therefore, for a homogeneous glass, light transmitted perpendicular to the glass leaves the glass with an angle perpendicular to the glass.

In the situation where the incident light travels from glass into air, i.e., when light leaves the glass, Snell's law is expressed as, Eq. (2.3).

$$\frac{\sin \theta_{\text{glass}}}{\sin \theta_{\text{air}}} = \frac{n_{\text{air}}}{n_{\text{glass}}} \Rightarrow \frac{\sin \theta_{\text{glass}}}{\sin \theta_{\text{air}}} = \frac{1}{n_{\text{glass}}} \quad (2.3)$$

From Eq. (2.3) it can be seen that for large angles of the incident light ( $\theta_{\text{glass}}$ ),  $\sin \theta_{\text{air}}$  should be larger than 1 to satisfy Snell's law. Since this requirement is impossible to fulfil, the light is refracted. The angle at which the total reflection sets in is denoted the critical angle ( $\theta_c$ ) and can from Eq. (2.3) be determined as:

$$\theta_c = \sin^{-1} \left( \frac{1}{n_{glass}} \sin \theta_{air} \right) = \sin^{-1} \left( \frac{1}{n_{glass}} \right) \quad (2.4)$$

By varying the angle of the incident light, the critical angle  $\theta_c$  can be determined and from this angle, the refractive index of the glass can be calculated. Reflection occurs at angles larger than  $\theta_c$ .

### Absorption

Absorption of light occurs when species in the glass absorb the incident light. When electrons absorb the energy of the light, they are excited to a higher energy binding state. Since, the electrons are excited to a certain binding shell, only light with a specific energy can excite the electrons. This implies that only certain wavelengths of the light are absorbed by a given species. Due to the nature of the absorption, it depends on both the element in question and its oxidation state.

### Transmission

The amount of light that is transmitted through a glass depends on the extent of reflection, refraction and absorption. Reflected and absorbed light are not transmitted through the glass. Refracted light is penetrating the glass, but since the angle of the light changes, two possibilities exist. Either, the refraction is strong and consequently, the light does not reach the detector or for small refractions, the light is refracted to certain parts of the detector which therefore appear brighter (Figure 2.8).

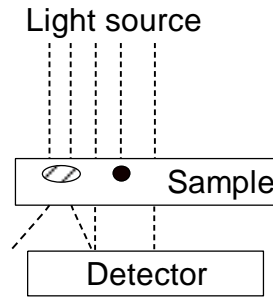


**Figure 2.8:** Schematic illustration of how a stria with a refractive index different from that of the glass matrix (the hatched area), refracts the light and how the transmission is affected by a stria which completely absorbs the incident light (the black area).

From Figure 2.8 it is evident that both changes in refractive index and absorption across the sample impact the signal received by the detector. Thus, a setup based on the illustration in Figure 2.8 is sensitive to striae in glasses.

The transmission ( $T$ ) of a glass is influenced by the thickness of the glass ( $l$ ) according to the Lambert-Beer law:

$$T = 10^{-\epsilon lc} \quad (2.5)$$

Where  $c$  is the concentration of species and  $\epsilon$  is the extinction coefficient.  $\epsilon$  is a constant which depends on the species in question, i.e., the chemical composition of the measured volume [Stolper 1982; Davis et al 1996]. Therefore, an inhomogeneous glass possesses a distribution of extinction coefficients. Since each stria can have its own chemical origin, it is not possible to determine the extinction coefficient for each of the domains in the glass. Therefore, the extinction coefficient of the entire glass is set to unity, i.e., a mean value is utilised for all domains in the glass. In the glass, species enriched in some striations are consequently depleted in others, i.e., the distribution of extinction coefficients is symmetrical around a mean value. Therefore, it

is reasonable to assume a uniform extinction coefficient for the entire glass. In the glass, the real extinction coefficient is a distribution around the mean value, which implies that some striae have a higher extinction coefficient than the mean extinction coefficient whereas other striae have a lower extinction coefficient than the mean. Consequently, the impact of some striae on the optical transmission of the glass is reduced whereas other striae contribute with an overestimated effect when all striations are assumed to have the same extinction coefficient. However, upon measurement of the transmission of the entire glass this error is removed. Upon measurement of the transmission and the thickness of the glass,  $c$  can be determined from Eq. (2.5).

#### 2.4.2 Processing of transmission data

Since dissolved raw material which partly has diffused into and mixed with the surrounding glass melt is responsible for the generation of chemical striae, the intensity of the striae changes in a continuous manner from the glass matrix to the centre of the striae. Furthermore, this continuous change in the striae intensity is symmetrical around the striae when the stria is surrounded by a homogeneous melt. In other words, the transmission around a stria is expected to change in an oscillating motion. Data sets with the measured parameter fluctuating in an oscillating motion can be analysed by Fourier transformation.

The Fourier integral can describe a set of data by fitting a function  $f(x)$ , which consist of cosine and sine contributions according to Eq. (2.6).

$$f(x) = \int_0^{\infty} [A(\omega) \cos(\omega x) + B(\omega) \sin(\omega x)] d\omega \quad (2.6)$$

where  $w$  is the angular frequency of the oscillation,  $x$  is the angle and  $A(w)$  and  $B(w)$  are trigonometric functions [Kreyszig 1999]. To simplify the analysis, it is common to use either sine or cosine terms. As frequency is the reciprocal dimension,  $w$  is the parameter that describes the dimension of the striae. The parameters  $A(w)$  and  $B(w)$  determine the weight of each  $w$  to the function. In other words, they are a measure of the how much each striae dimension contributes to the output signal (the stria intensity). After fitting Eq. (2.6) to a given data set, the signal (which is later denoted amplitude), is obtained as a function of frequency of the striae oscillation (reciprocal dimension of the striae).

### 2.5 Characterisation of bubbles

As an important and prevalent type of inhomogeneity, bubbles have attracted the interest of glass scientists and technologists for decades. Since bubbles are chemically and physically very different from the glass, detection of bubbles can be achieved by several means. Due to the large differences in the chemical and physical properties between a bubble and the surrounding glass, bubbles are detectable by visual inspection. To detect bubbles that remain hidden to the naked eye, optical microscopy can be applied as bubbles appear on images acquired by optical microscopy.

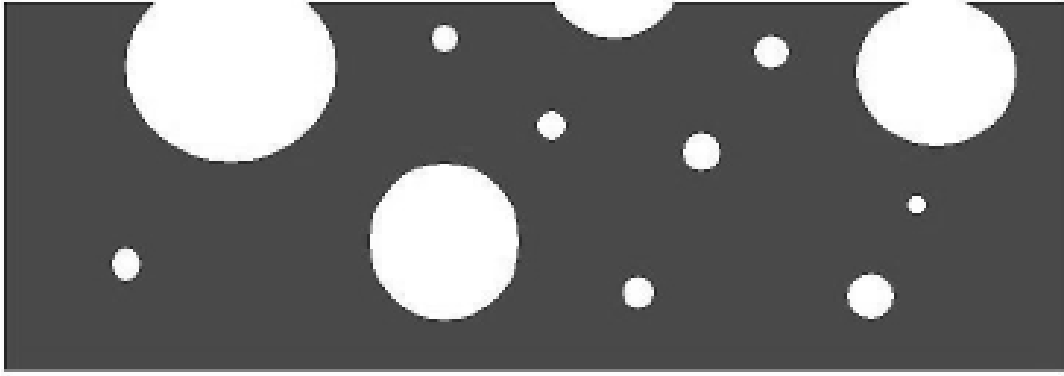


**Figure 2.9:** Cross section of a bubble containing glass.

Figure 2.9 shows a cross section of a bubble containing glass. An inspection of the glass surface reveals the presence of bubbles, but the observed bubble diameter is smaller than true diameter of the bubble. This phenomenon is caused by the spherical nature of the bubbles, i.e., the true diameter of the bubble is only visible when the core of the bubble appears on the acquired image. In other words, a quantification of bubble sizes or bubble volume by analysis of surface images contains a systematic error. Although mathematical corrections for the systematic error have been proposed, it is desirable to measure the bubble diameter by a method which excludes the systematic error. A stack of 2D images (a kind of 3D image) has two advantages compared to ordinary 2D images of the sample surface. First, the core of the bubble can be identified and at this position the true diameter of the bubble can be found. Second, image stacks contain information from a large volume compared to a 2D image, which reduces the statistical uncertainty. This is of particular importance for bubble volume determination since it can be strongly affected by a few large bubbles.

## 3 Characterisation of striae and bubbles

### 3.1 Characterisation of striae

Optical transmission analysis of images has the advantage over ordinary transmission measurements that the measurement is orders of magnitudes faster. The fast acquisition rate enables sampling of large amounts of data and a concomitant low statistical uncertainty. Furthermore, a spectrometer normally employed for transmission measurements has a fixed spot size, usually in the range of 0.5 to 2 mm, i.e., the resolution of the transmission measurement is fixed and rather larger. For image analysis, the image can be acquired in reflection or transmission mode and by means of different techniques, e.g., by a digital camera or an optical microscope, depending on the size of the structures of interest. Furthermore, the various image acquisition techniques have different contrast sensitivities, i.e., some techniques such as interferometers can detect very weak striations. In this work, it is decided to acquire the images by means of a scanner since this technique covers the size range where most striae are found. Depending on the applied scanner, it is possible to detect striae from  $\sim 10 \mu\text{m}$  to  $\sim 20 \text{ cm}$ , i.e., 4 orders of magnitude with respect to size are covered by a scanner.

#### 3.1.1 Image acquisition

In order to make the visible light transmission of glass detectable, the sample must be optically transparent. Thus for highly absorbing samples such as iron-bearing glasses, the sample must be ground and polished to a thickness, where light can be transmitted through the glass. The transmission ranges from 0 to 100 % and during the digitalisation, which occurs during the image acquisition, the absolute transmission is converted into a grey scale. The absolute transmission can be converted to either 8 or 16 bit grey scale (Figure 3.1).

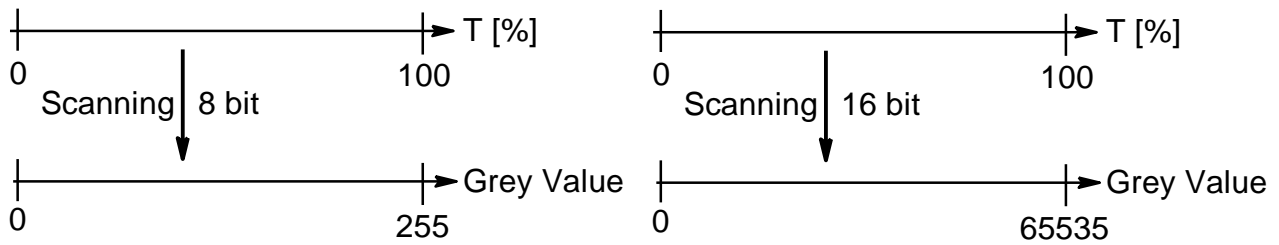


**Figure 3.1:** Conversion of absolute transmission to grey scale during image acquisition.

Scanning in 8 bit mode converts the absolute transmission into 256 grey values, whereas 65536 grey values describe the transmission in 16 bit mode. Therefore, scanning in 16 bit mode provides a better precision and an improved detection limit compared to 8 bit mode. During scanning of the glass sample, the brightness and the contrast of the image can be adjusted to fit the transmission of the sample. Hence, instead of including the entire transmission spectrum from 0 to 100 % a part of the spectrum can be selected and converted to the grey scale as illustrated for 8 bit mode in Figure 3.2.

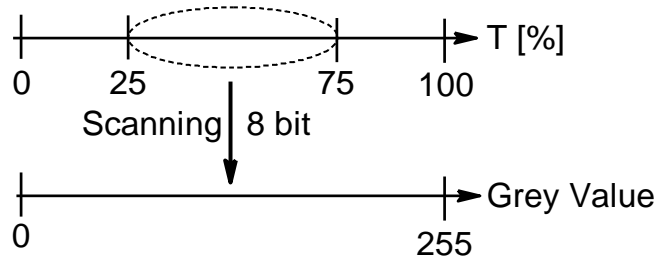


**Figure 3.2:** Conversion of absolute transmission to grey scale during image acquisition when the scanning brightness and contrast are optimised for the sample in question. In this example the transmission range 25 to 75 % is scanned.

When the brightness and contrast are optimised to each sample, the detection limit and precision are improved. When the entire transmission range is scanned as in Figure 3.1, each per cent change in transmission is described by 2.5 grey values. If the scanned transmission range is restricted to the transmission range of the sample, as exemplified with the range 25 to 75 % in Figure 3.2, 5 grey values cover one per cent change in transmission.

To strengthen the physical foundation of a stria characterisation based image analysis, it is desirable to reconvert the grey values into absolute transmissions. This reversion can be achieved through the utilisation of a calibration sheet. The calibration sheet contains domains with various, but well-defined transmissions. Hence, by scanning the calibration sheet with the same settings as the sample, the grey values of the sample can be converted to an absolute transmission (Figure 3.3).

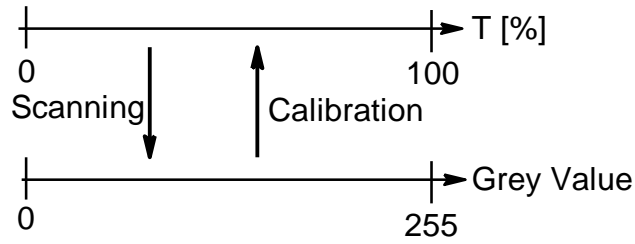


**Figure 3.3:** The initial scanning of the sample converts the absolute transmission of the sample into grey values. Through a calibration sheet, the grey values of the sample can be reconverted to absolute transmissions.

The relationship between the absolute optical transmission and the grey scale is described by a power law where the gamma value is the exponent in the power law. Therefore, when scanning the glass samples with a gamma value of 1, a linear relationship between the absolute transmission and the grey values is obtained. Hence, by scanning the calibration sheet with the same settings as the sample, the equation for the linear relationship between the absolute transmission and the grey values can be obtained.

A sample contains striae residing in different depths of the glass sample. During the image acquisition the striae in the glass volume are projected onto the 2D image. A projection can inflict sampling errors if striae are residing in different depths on the same area of the glass. However, for thin glass samples and glasses of low stria content, the projection is not expected to introduce any systematic error to the stria characterisation.

### 3.1.2 Image processing

In bubble containing glasses, the bubbles have a large impact on the stria characterisation since bubbles also exhibit a contrast difference to the parent glass. To remove the effect of bubbles on the stria characterisation, bubble containing images undergo an initial processing before the image analysis can be conducted. To perform the image processing, the freeware ImageJ is used [Abramoff et al 2004]. The software offers several

useful functions and the possibility to write own macros to automatize repeatable actions. The effect of the bubbles can be eliminated by substituting the bubble representing pixels on the image with the average grey value of the glass representing pixels. To perform this substitution, ImageJ must be capable of distinguishing between bubbles and glass. In practice this is achieved by colouring all the bubbles of the image black.

The first step in the colouring process is to duplicate the original image in order to compare an image, where the bubbles are coloured black, with the original image. Hence, the bubble colouring process is only performed on one of the two images. To colour the bubbles black, the rim of the bubbles is identified by its contrast difference to the surrounding glass by means of the “Find Edges” function. Subsequent to the identification of the position of the bubbles on the image, the modified image is made binary (i.e. all pixels on the pixels on the image are made purely white or black) with the “Make Binary” function. To make the entire bubble appear black on the binary image, the core of the bubble is coloured black by choosing “Fill Holes”. Finally, the modified image is subtracted from the original one using the “Image Calculator” function. On the resulting image, all bubbles are completely black, whereas all other areas are unaffected by the processing. As the bubbles appear completely black, they are easy objects to recognise. By means of the “Remove Outliers” function, the bubbles (dark outliers) can be removed from the image by adjusting two parameters: radius of the objects and the grey value threshold of the objects that should be replaced. The radius depends on the size of the bubbles on the image. The appropriate grey value threshold is found by measuring the grey value median of the image by applying the functions “Select All”, and then “Set Measurements” with the median marked. By choosing “Measure”, the grey value median of the image is found. The grey value threshold is set to  $1/3$  of this median, i.e., pixels with a grey value that more than  $1/3$  below that of the median are replaced if they are within the radius criterion. After removal of outliers, the bubbles representing pixels have been substituted with the median grey value of the image.

### 3.1.3 Line scanning

Since striae are a continuous fluctuation in the transmission of the glass (section 2.4), it is necessary to measure the optical transmission at a successive number of points instead of measuring it at randomly selected single points. In practice this is obtained by measuring the grey value along a line on the image, i.e., by so-called line scanning. In order to compare the striation extent of different glasses, it is necessary to employ a fixed line length since a longer line length in the line scan enables the detection of transmission fluctuations over larger lengths (i.e. larger striae). Therefore, glass analysed with a larger line length during the line scan appear more inhomogeneous than those analysed with a shorter line length.

During line scanning, the optical transmission expressed as grey value is determined. Through the linear relationship between transmission and grey value in addition to measurement of the glass thickness, the concentration of striae ( $c$ ) can be determined from Eq. (2.5). This algorithm is written into the self-build line scan macro, which records the grey value along a line with a certain length and then recalculates the recorded grey values to striae concentrations. Thus, the striae concentration is determined along the inserted line.

For bubble containing glasses, the line scanning is conducted on the image where the bubbles have been replaced with the median grey value of the glass matrix and for non-bubble containing glasses, the line scanning is performed on the as-acquired image. To eliminate systematic and statistical errors, a macro for automatic and random selection of the line scanning domain is constructed. Furthermore, 500 lines scans are performed on each image.

### 3.1.4 Fourier transformation

The 500 line scan files, each with a fixed amount of striae concentration points, are loaded into the program Qtiplot. A self-written script automatizes the Fourier transformation for each of the line scans. Upon Fourier transformation of each line scan, the script ensures calculation of the average of all 500 Fourier transformations. Thus, the outcome of the Fourier transformation is the average amplitude at different frequencies (in inverse pixels) and the standard deviation of the amplitude. By accounting for the resolution of the image acquisition the unit of the frequency is converted from  $\text{pixel}^{-1}$  to  $\text{m}^{-1}$ .

## 3.2 Quantification of bubble size

Similar to the stria characterisation, the bubble analysis is performed on images. However, whereas the stria characterisation is performed on 2D images, the bubble analysis is performed on stacks of 2D images. Due to the similarities between the approaches, the quantification of bubble size involves three steps: image stack acquisition, image processing and image analysis.

### 3.2.1 Image stack acquisition

The depth images required for a 2D stack can only be obtained by operating the microscope in transmission mode, i.e., the inspected sample must transmit light. Furthermore, the microscope must feature an automatic z-stage, i.e., the height of the stage (and consequently the focus of the microscope) can be adjusted and controlled precisely. A random area is selected for investigation and the focus of the microscope is set  $30\text{ }\mu\text{m}$  below the surface of the sample to avoid potential dirt and scratches on the sample surface. Upon measurement of the selected area, the z-stage is moved to shift the focus to a deeper layer in the sample. The distance between each of the layers in the z-dimension is denoted the depth resolution. The acquisition of an image of one layer followed by a change of the focus is continued until an image stack with the desired depth is obtained. Since the focus is adjusted in discrete steps, the resolution of each 2D image is in most cases better than the depth resolution. Since the argument for choosing analysis of 2D stacks is the fact that the true bubble diameter solely can be determined at the centre of the bubble, the required depth resolution depends on the size of the bubbles. This implies that large bubbles can be measured with a poorer depth resolution than small bubbles. To reduce the statistical uncertainties, 2D stacks are acquired from four domains of the sample.

### 3.2.2 Image processing

To improve the bubble counting accuracy, the 2D image stacks are initially processed through a series of steps in ImageJ. During the bubble counting procedure, the bubbles are recognised through their shape and contrast difference to the surrounding glass matrix. However, since striae also possess a contrast difference to the parent glass, it is desirable to remove some of the striae prior to the bubble counting. This is achieved by the “Bandpass Filter” function. Structures above a certain size and structures below a certain limit can be removed. Hence, the lower limit can be set to a few pixels to remove noise, whereas the upper limit must be larger than the largest bubble that should be detected. In addition to the lower and upper size threshold, “Suppress Stripes” is set to none, “Tolerance of direction” is 5 %, “Autoscale After Filtering”, “Display Filter” and “Saturate Image when Autoscaling” are disabled. To have a clearer appearance of the bubbles on the image, the background of the image is subtracted from the image by means of the “Subtract Background”

function. For this process the parameter “Rolling Ball Radius” is adjustable. This parameter determines the fineness of background subtraction. Thus, a large “Rolling Ball Radius” tends to blur the image and therefore impedes the bubble counting. Since the bubble counting function detects bright objects, it is necessary to invert the image, i.e., bright areas are converted to dark ones and vice versa. The last step of the image processing applies the “Enhance Contrast” function where the parameter “Saturated Pixels” determines the extent of the contrast enhancement. The value determines the number of pixels that become either completely white or black and is in this work set to 0.5 %. The option “Normalize all Slices” is checked so the grey value range is maximised after the contrast enhancement, i.e., grey values from 0-65535 are present on 16 bit images. If “Normalize all Slices” is disabled, the grey values of the image are not recalculated after the contrast enhancement and consequently, the contrast difference between bubbles and glass is smaller.

### **3.2.3 Image analysis**

To count the bubbles, the “object counter 3D plugin” is used [Bolte & Cordelières 2006]. The plugin contains a contrast threshold variable. The operator must decide the threshold grey value that excludes unwanted objects without excluding bubbles from the detection. The plugin recommends a threshold, which in most cases is very close to the operator’s assessment. After adjustment, the computer detects objects that satisfy the contrast threshold requirements and determine position, shape and volume of the objects. Commonly, some non-spherical objects are erroneously detected during the bubble counting. However, since the shape of each object is determined, these unwanted, non-spherical objects can be identified and excluded from further data processing.

## 4 Characterisation of inhomogeneities

### 4.1 Stria characterisation

#### 4.1.1 Characterisation of simulated striations

In order to test whether Fourier Transformation of transmission measurements performed on images is a feasible method for the characterisation of striae, a simple stria simulation is initially considered. A glass with well-defined striations is modelled by constructing an image that gradually changes from completely black (grey value of 0) to completely white (grey value of 255) over a length of 100 pixels (see paper 1 for details). The ideal striation and line scan on the striated image are shown in Figure 4.1.

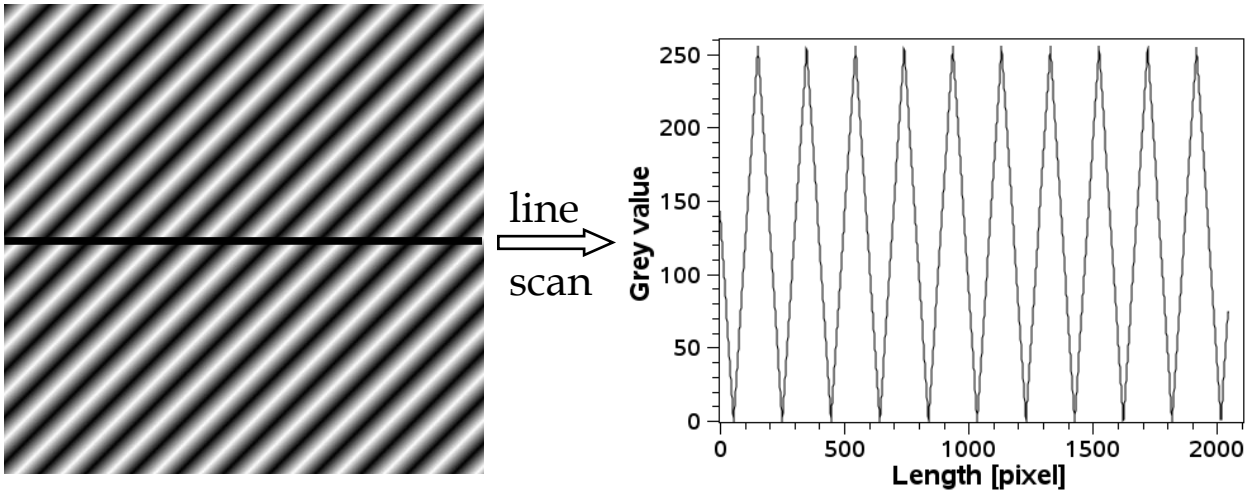


**Figure 4.1:** The simulated striation and the line scan conducted at the black line inserted in the image.

From the line scan of the simulated striation, it is observed that the grey value fluctuates between 0 and 255 over a length over 100 pixels, which is similar to the input parameter of the model. Hence, the line scanning can characterise the grey value changes of the model. To describe the periodicity and the amplitude of the grey value changes, the line scan is subjected to Fourier Transformation (Figure 4.2). In the Fourier Transformation spectrum, the amplitude is a measure of the grey scale intensity change, i.e., a measure of the extent of the grey value change.

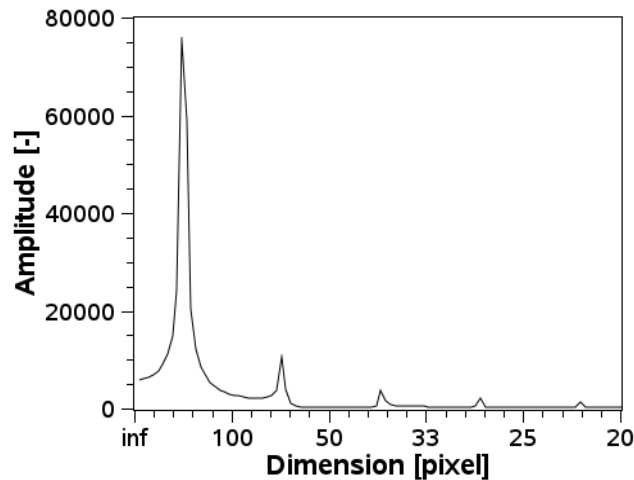


**Figure 4.2:** Fourier transformation spectrum of the line scan on the simulated striation. The amplitude of the fitted sinus curves is plotted as function of their dimensions (1/frequency).

In the Fourier Transformation spectrum, several peaks can be observed. The largest peak occurs at 200 pixels, which reflects the distance in the modelled striation between a completely black pixel and the next completely black pixel, i.e., a peak in the Fourier Transformation spectrum is obtained at the dimension corresponding to the oscillation period of the stria. The minor peaks in the Fourier transformation spectrum are artefacts from the simulation. In the simulated striation, the grey value changes abruptly (discontinuously) at the maxima and minima (see Figure 4.1). The harmonic sine curves are applied in the Fourier transformation exhibit a continuous change at the maxima and minima. Therefore, the discontinuous changes in the grey value of the simulated striation are in contradiction with the nature of the harmonic oscillations used in the Fourier transformation. Hence, a single sinus curve with a period of 200 pixels cannot describe the periodic structure of the simulated striation. To describe an abrupt change in grey value as a function of the position, it is necessary to incorporate sinus functions with higher frequencies (shorter dimensions) into the Fourier transformation signal. These extra sinus functions with higher frequency are seen as the minor peaks at 67, 40, 29, and 22 pixels. These dimensions match the odd harmonics of the major sinus function at 200 pixels, i.e., the odd harmonics are 3, 5, 7, and 9 times shorter than the major sinus curve with a period of 200 pixels. By adding these extra terms to the major sinus curve, it is possible to describe the sudden changes in the grey value at the maxima and minima. Since real glasses contain striae of different sizes and orientations, a Fourier transformation spectrum contains broad peaks at several dimensions, which complicates the interpretation of the spectrum. Therefore, the Fourier transformation spectrum is integrated over dimension (Figure 4.3).

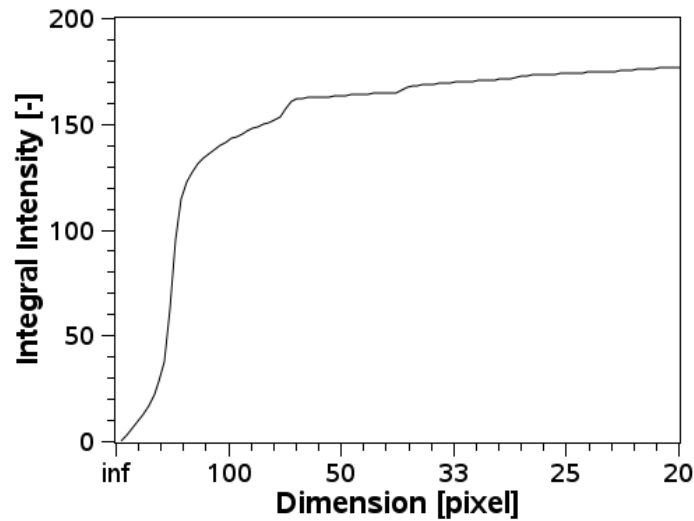


**Figure 4.3:** The integrated Fourier transformation signal of the simulated striation.

In the integrated Fourier transformation spectrum, the integral intensity increases significantly at 200 pixels demonstrating the presence of striations with a size of 200 pixels. These 200 pixels represent the stria size in the simulation and are similar to the dimension exhibited in the Fourier Transformation spectrum (Figure 4.2). At dimensions below 200 pixels, the intensity continues to increase with decreasing dimension, due to the higher frequency sinus curves required to fit the sudden grey value changes at the maxima and minima. However, when inspecting real samples, the small peaks from the odd harmonics are not present since grey value changes occur gradually in real striae. This implies that the oscillations of the transmission caused by real striae better resemble those of a sinus curve as discussed in detail in paper 1.

#### 4.1.2 Characterisation of glasses from stone wool melts

To investigate the applicability of the stria characterisation method on real glasses, samples from stone wool melts produced by means of three different furnaces technologies are subjected to the image analysis. The images of each of the three samples from the different furnaces are shown in Figure 4.4.

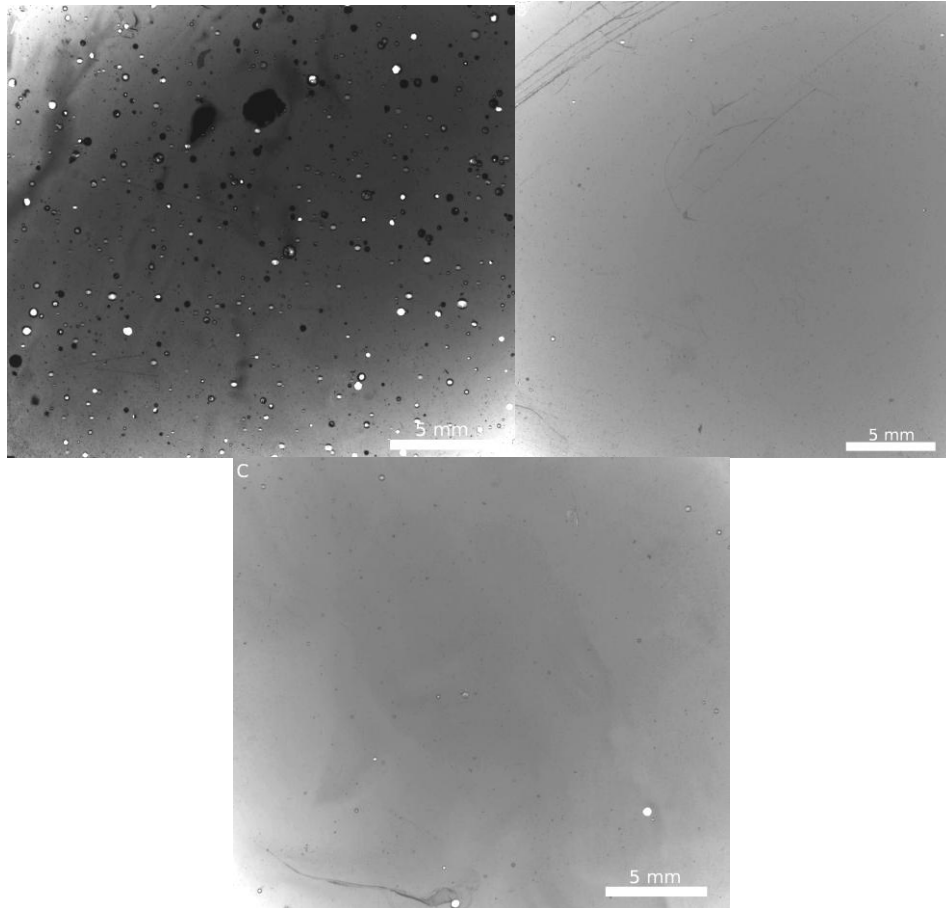


**Figure 4.4:** Images of a sample from each of the three different furnaces technologies. A: cupola furnace, B: electric furnace, C: test furnace. The brightness of the images is optimised for printing.

From the images of the samples it is clear that besides striae the glasses contain bubbles, in particular the glass from the cupola furnace (Figure 4.4). Similar to striae, a contrast difference between a bubble and the surroundings glass matrix is present. Since the contrast difference between a bubble and the glass is larger than that between a stria and the glass, bubbles appear as very intense striations in the line scanning. Consequently, the presence of bubbles causes a systematic error in the stria characterisation. To avoid the effect of bubbles on the stria characterisation, the bubbles are prior to the line scanning removed from the image by means of image processing (paper 2). During the image processing, the bubble representing pixels are replaced by pixels with the median grey value of the image, i.e., the contrast difference between the bubble and the glass vanishes. The integrated Fourier transformation curves of the samples from the three different furnaces used in the production of stone wool melts are shown in Figure 4.5.

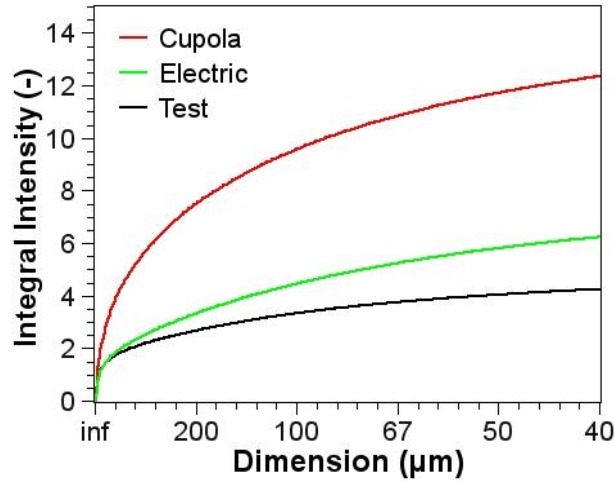


**Figure 4.5:** Integrated Fourier transformation curves for stone wool melt samples where the bubble representing pixels have been substituted with the grey value median of the glass on the acquired images. For the analysis a line length of 2500 pixels (19.8 mm) has been applied for the line scan.

For all three samples, the integrated intensity increases continuously with decreasing dimension, but the rate of the increase declines as smaller dimensions are approached and at about 40  $\mu\text{m}$ , a constant slope is found. Unlike the simulated striae, there are no abrupt changes in the integrated intensity for the striae in the glasses as striae with various dimensions are present in real samples. The intensity is highest for the cupola sample, which implies that the contrast differences are larger on this image than the others. The larger intensity of the cupola sample is supported by a visual inspection of the image (Figure 4.4). Since there are no abrupt increases in the integral intensity, quantities for describing the striae in the sample must be obtained by other means than visual inspection of the integrated Fourier transformation curve. To obtain such characteristic quantities, two tangent lines are constructed from the integral intensity curve. The first line is plotted from the linear part below  $\sim 40 \mu\text{m}$ , whereas the second line is plotted at the linear part at larger dimensions as illustrated for the cupola sample in Figure 4.6.

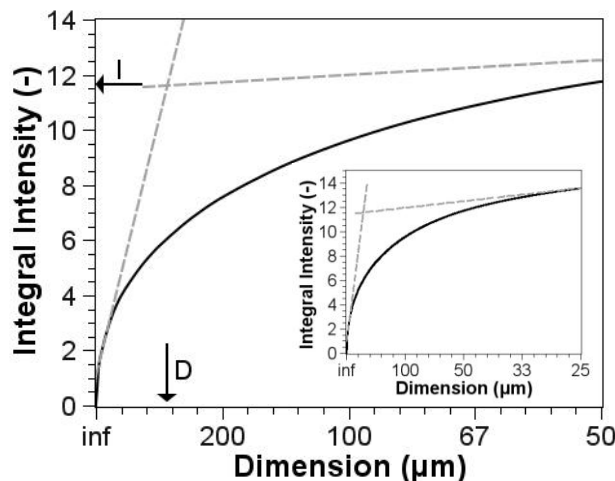


**Figure 4.6:** The integrated curve and the two tangent lines used for the determination of the two characteristic values ( $D$  and  $I$ ). The integrated curve is from the glass sample taken from the cupola furnace. The ordinate is rescaled in the inset to show the origin of both tangent lines.

The intersecting point of the two tangent lines is used as a measure of the extent of the striations in the glass. The abscissa value at this point represents the characteristic striae dimension (a quantity describing the striae

size distribution) in the melt, while the ordinate value is a measure of the striae intensity (a measure of the transmission difference between the striae and the surrounding matrix). In other words, the striations are characterised by the two independent quantities reflecting the intensity (the degree of chemical fluctuation) and the size of the striations. The characteristic intensity ( $I$ ) and dimension ( $D$ ) of the samples from the three different furnaces are listed in Table 4.1.

**Table 4.1:** The characteristic intensity ( $I$ ) and dimension ( $D$ ) for stone wool melt samples produced by means of different furnace technologies.

	$D$ ( $\mu\text{m}$ )	$I$ (-)
Cupola	355	11.6
Electric	408	5.76
Test	471	3.99

$D$  is smallest in the cupola sample implying that small striae constitute a larger part of the total striae fraction. In both the cupola and electric furnace, lumps of raw materials are loaded into the furnace, but the retention time is 10 to 20 times longer in the electric furnace than in the cupola furnace. During the melting process, striae are equilibrated through diffusion. Since small striae are equilibrated faster than the larger ones, some of the smaller striae have been equilibrated in the sample from the electric furnace. As a consequence, some of the small striae have vanished in the sample from the electric furnace whereas the large striations remain in the melt. The equilibration of the small striae in the electric furnaces is reflected by the characteristic dimension ( $D$ ).  $D$  is larger in the sample from the electric furnace than in the sample from the cupola furnace, i.e., the striae size distribution is shifted to larger dimensions in the electric furnace. In addition, the large intensity of the cupola sample emphasises that only limited diffusion occurs during the melting process in this furnace. The test furnace has the highest dimension and the lowest intensity, i.e., it is the most homogeneous of the three samples. Since the test furnace operates under conditions different from those of the two other furnaces, it is difficult to relate the characteristic values of sample from the test furnace to the characteristic values of the two other samples.

Since the results presented in paper 1 are obtained by the use of a different line length than the one used for the determination of the characteristic parameters presented in Table 4.1, the results are not directly comparable. Furthermore, the characterisation presented in paper 1 has not been performed with conversion of grey values to absolute transmissions. A relative comparison between the two studies is, however, possible. In paper 1 the two characteristic quantities of the sample from the test furnace is similar to those of the sample from of the cupola furnace, whereas the test furnace sample is the most homogeneous one according to the characteristic values in Table 4.1. The test furnace sample utilised in the paper 1 is taken at a point where the furnace was in its start-up phase whereas the sample from the test furnace shown in Figure 4.4 is taken after optimisation of the furnace. The optimisation of the test furnace is reflected by a higher characteristic dimension and a lower intensity.

### 4.1.3 Discussion of the stria characterisation method

In contrast to other methods for stria characterisation such as the Christiansen filter method (subsection 2.3.1) and refractive index measurements (subsection 2.3.3), the image analysis method can provide independent measure of striae intensity and dimension. The light refraction changes detected by the Christiansen filter method depend on both the refractive index difference and the thickness of the striated domain. In other words, the Christiansen filter method provides a quantity of light refraction change, which relies on two parameters: the chemical gradient and the thickness of the striated region. In the present method, the

integral intensity is the sum of the transmission difference at a given dimension. Hence, many mild striae provide the same signal as a few intense striae, i.e., it cannot be defined from the new method whether the integral intensity arises from a few intense striae or several milder ones. Unlike, the Christiansen filter method and refractive index measurements, it is, however, possible to discriminate between striae intensity and size. Finally, as the new method measures the optical transmission of the glass, it addresses both striae with a refractive index gradient and striae with a gradient in visible light absorbing species. Whereas any change in the chemical composition leads to a gradient in the refractive index, the visible light absorbing striae only arise from gradients in certain species. Changes in the light absorption occurs if the concentration of the light absorbing species fluctuates or if the redox state of the light absorbing species varies across the glass. Hence, for stone wool melts, a chemical gradient in the iron oxide concentration and differences in the iron oxidation state inflict a stria with a visible light absorption different from that of the glass matrix.

In real samples, a distribution of striae dimensions exists. Due to the irregular shape of striae, it is not possible to describe a stria by a single dimension. In addition to the complex shape of striae, the part of the striae measured by the line scan is randomly selected. As a consequence of the random selection of the line scanning domain, even line scan of a square exhibits various dimensions as illustrated in Figure 4.7

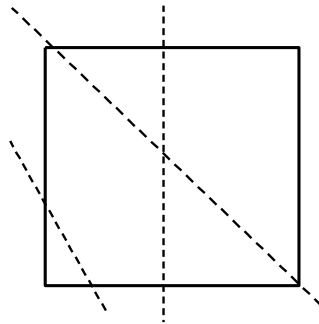


**Figure 4.7** A striated region (the square) where three line scans (dashed lines) at randomly chosen positions are conducted.

The randomly positioned line scans in Figure 4.7 result in different striae dimensions. In other words, for randomly conducted line scans, even well-defined structures exhibit a broad size distribution in the Fourier transformation spectrum. However, since real striations have a complex shape, it is not possible to define a certain dimension for a stria. The exact measure of the size of a stria is the volume of the stria. Such measurement requires the determination of a boundary between the stria and the glass matrix, i.e., criteria for the determination of the threshold for the boundary must be found. The advantage of the present method is the ability to describe continuous change of the chemical composition (and hence transmission).

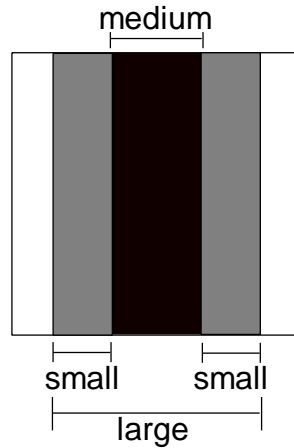


**Figure 4.8:** A stria in a homogeneous glass matrix (the white part). The stria consists of two domains with a small chemical composition difference to the glass matrix (grey area) and a core (black area) with a large chemical composition different to the glass matrix. For a line scan conducted perpendicularly on the stria, the length of each of the domains in the stria is given.

In Figure 4.8, a homogeneous glass matrix (white area) contains a stria with two domains (grey and black areas). The first outer domain (grey areas) has a smaller chemical composition difference to the matrix than the inner domain (black area). A line scan perpendicular to the stria results in a Fourier Transformation spectrum with 3 peaks. The peak with the largest dimension (length marked as “large” in Figure 4.8) represents the entire length of the striae. The peak at the medium dimension arises from the black core. The peak at the smallest dimension arises from the two grey areas. Consequently, a stria with various changes in the chemical composition (i.e., transmission) is split up into sub parts during the Fourier transformation to characterise the stria. This splitting circumvents the problem of defining a boundary between the striae and the surrounding glass.

During the determination of the characteristic quantities, the largest uncertainty is associated with the dimension. The uncertainty arises since the Fourier Transformation determines the amplitude as a function of frequency (reciprocal dimension). Since the characteristic dimension occurs at a low frequency, small changes in the frequency at the intersection point of the two tangent lines have a rather large effect on the characteristic dimension. The axis of the integral intensity is linear and therefore the characteristic intensity is only affected to a minor extent by changes in the intersection point of the two tangent lines.

## 4.2 Ranking the homogeneity of glass

Nowadays thousands of technical glasses and daily life used glasses exist. Due to the large span in the application of glasses, their homogeneity differs significantly. As an example, comparison of the glasses from stone wool melts shown in Figure 4.4 and a window glass reveals that the window glass is the most homogeneous one. Similarly, it is obvious that a glass used as lens in a microscope is more homogeneous than a bottle glass. To move beyond these straight-forward qualitative comparisons to a solid scientific comparison of the homogeneity of different glasses, a methodology for a quantitative description of glass homogeneity must be established. Therefore, the new method is applied to characterise the striae in different glasses and it is explored whether the method can rank the homogeneity of different glasses.

As homogeneity is an issue that covers several aspects such as striae, bubbles and undissolved raw materials, it is necessary to select a certain type of inhomogeneity for the ranking. Stone wool melts contain striae, bubbles and to a minor extent undissolved raw materials, but in other glasses the presence of undis-

solved raw materials is very rare. Furthermore, bubbles are only present in limited numbers in other glasses. Therefore, a ranking of the homogeneity of a wide selection of glasses is conducted from a characterisation of the striations in the glasses.

To study the applicability of the stria characterisation method on other glasses and the rank the homogeneity of inorganic glasses in general, various glasses are selected. For the ranking, 7 industrial glasses and 6 fluoride and oxyfluoride glasses produced at laboratory scale are selected. Since all glasses in the study are more homogeneous than the glass from the stone wool melt, it is necessary to perform the image acquisition and processing in 16 bit mode. 8 bit mode is sufficient to characterise the intense striae in the glass from stone wool melts, but for more homogeneous glasses an improved detection limit is required, which is achieved by conducting the stria characterisation in 16 bit mode (see detailed discussion in subsection 3.1.1). The striae analysis of a green bottle glass (Bottle G), a lead “crystal” glass (Lead), a window glass (Window) and the K9 optical silicate glass (K9) is shown in Figure 4.9.

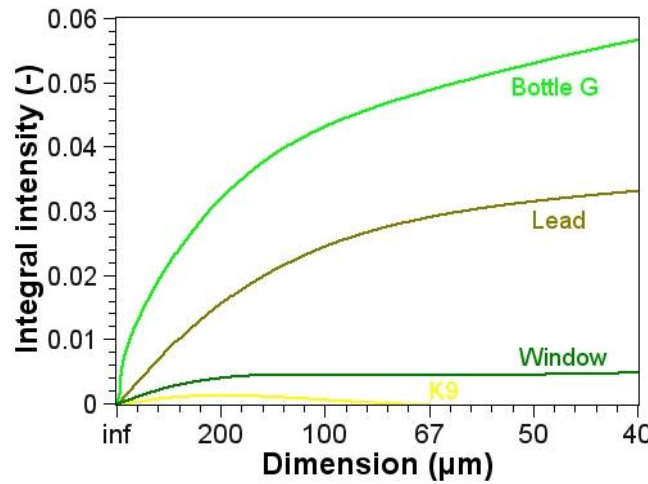


**Figure 4.9:** Striae analysis of a green bottle glass (Bottle G), a lead “crystal” glass (Lead), a window glass (Window) and the K9 optical silicate glass (K9). The stria analysis is performed on images acquired in 16 bit mode.

Since the stria analysis of the four glasses in Figure 4.9 is conducted in 16 bit mode, the integral intensities cannot be compared with those in Figure 4.5. The shape of each of the curves in Figure 4.9 is different, reflecting a different striation pattern in each of the samples. During the scanning procedure, the samples are placed on a transparent foil on the scanner as direct contact between the glass sample and the glass surface of the scanner leads to reflection of the incident light. For the striae analysis, the difference between the line scans performed on an image of the transparent foil and line scans performed on an image of the sample on the transparent foil is determined. The intensity of the K9 glass fluctuates around 0, i.e., the transmission changes in the sample is similar to that of the transparent foil. In other words, it is not possible to detect any striations in this glass since the intensity of any possible striations is below the detection limit of the scanner. For the window glass, the integral intensity increases at high dimensions and is then constant at low dimensions. The trend of the integral intensity curve of the window glass reflects that this glass only contains large striae. Just after the liquids temperature of the batch has been exceeded in the melting process, it is likely that striae exist in the melt. In a glass melt with large striae, small striae must be present as well since large striae are caused by utilisation of large raw material pieces or poorly mixed batch and the small striae arise from a smaller raw material grains. In contrary small striae can exist in the melt without the presence of large striae if raw materials of a small size are used in a perfectly mixed batch. The small striae that initially were present in the window glass melt have been eliminated by diffusion. In the window glass, striae with a size below 200 µm have been completely eliminated and the intensity of the large striae has been reduced

during the melting process. For both the green bottle glass and the lead silicate glass, the integral intensity increases at all dimensions, which implies that these samples contain both large and small striae. The green bottle glass has the largest integral intensity, i.e., the largest transmission changes across the glass.

Unlike the three other glasses in Figure 4.9, the green bottle glass contains polyvalent elements, i.e., it can contain both absorption and refractive index induced striae. As absorption induced striae strongly affect the transmission of the glass, it is expected that the green bottle glass has a higher integral intensity than the three others. This is further supported by a higher homogeneity of the white bottle glass compared to the brown and green ones (paper 3).

To compare the stria characterisation by means of the image analysis method developed in this work with a known technique, refractive index measurements are performed on the same glasses. The refractive index ( $n$ ) and the standard deviation of the refractive index ( $\Delta n$ ) determined from 4 different spots on each glass are given together with the characteristic dimension ( $D$ ) and intensity ( $I$ ) in Table 4.2. These four values for all the glasses in the ranking study are listed in Table II in paper 3.

**Table 4.2:** Homogeneity measured by the scanner method and measurement of refractive index. The characteristic dimension  $D$  and the characteristic intensity  $I$  determined from the curves in Figure 4.9. Mean refractive index ( $n$ ) and refractive index variation ( $\Delta n$ ), given as the standard deviation of the refractive index of the sample, arise from the refractive index measurements.

	Bottle G	Lead	Window	K9
$D$ (mm)	0.115	0.103	0.269	-
$I$ (-)	0.0576	0.0337	0.0039	-
$n$ (-)	1.51274	1.54432	1.52252	1.51495
$\Delta n \cdot 10^{-5}$ (-)	11	9	9	13

Unlike the two quantities ( $D$  and  $I$ ) determined by the image analysis method, the standard deviation of the refractive index ( $\Delta n$ ) is almost similar for all four glasses. In fact, the refractive index measurements identify the optical silicate glass as the most inhomogeneous of the four glasses, which appears to be an erroneous finding. Therefore, it is concluded that the homogeneity of the glasses cannot be evaluated from refractive index measurements. The similar  $\Delta n$  values for the glasses can have two reasons. First, for the refractive index measurements, the spot size of the beam is a few hundred micro meters. The main difference between the window glass and the green bottle glass is the presence of striae with a size below 200  $\mu\text{m}$  in the latter glass as the integral intensity of the green bottle glass increases below 200  $\mu\text{m}$  whereas it is almost constant for the window glass at these dimensions (Figure 4.9). Due to the large spot size, striations below the size of 200  $\mu\text{m}$  cannot be detected and hence, the glasses cannot be distinguished from each other with respect to small striae when refractive index measurements are conducted. Second, time consumption of the refractive index measurements, limits the number of measurable spots on the sample, which causes a statistical uncertainty in the result. The analysis of images acquired by means of a scanner can discriminate between the glasses except for the optical silicate glass (K9), whereas the refractive index measurements are unable to rank the glasses with respect to their striations. Therefore, the ranking is performed on the results obtained from the image analysis method. To perform the ranking, the glasses are characterised by the homogeneity index ( $H$ ) which is defined as:

$$H = \log (D/I) \quad (4.1)$$

From Eq. (4.1), it is seen that  $H$  increases with increasing homogeneity since a homogenous glass is characterised by a large dimension and a small intensity. The two characteristic quantities of the all the samples in the ranking study are given in paper 3.

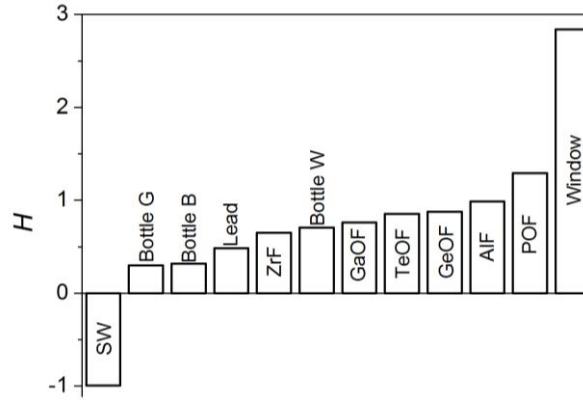


**Figure 4.10:** The homogeneity index  $H$  of the studied glasses. Since the homogeneity of the K9 is better than the detection limit of the scanner, this glass is excluded from the figure. The abbreviations of the glasses can be seen in paper 3.

The glass made from stone wool melt produced in the cupola furnace (SW) is clearly the most inhomogeneous of the investigated glasses since it is the only glass with a negative  $H$  value. The most homogeneous glass is the optical K9 glass, but as the homogeneity of the sample is beyond the detection limit of the scanner, quantification of its homogeneity cannot be performed. The window glass is the most homogeneous of the studied glasses within the detection limit of the scanner. The extent of the striations in this industrial product is smaller than that in the glasses produced at laboratory scale, which is a remarkable achievement. Obviously, the homogeneity requirements are higher for a window glass than for a bottle glass, but the high homogeneity of the window glass demonstrates that thorough optimisation of the melting process enables production of very homogeneous glass in furnaces with large throughputs. Disregarding the window glass, the glasses produced at laboratory scale are in general more homogenous than the industrial glasses.

To apply the utilised stria characterisation method to the very homogeneous optical glasses, a more accurate image acquisition technique is required. Such a technique could be interferometry, where refractive index changes down to  $10^{-7}$  (Puryayev 1998) or with a more complicated setup even down to  $10^{-8}$  can be measured (De Freitas & Player 1995). Through application of the image analysis used in this work on images acquired by means of interferometry, the striations in the highly homogeneous glasses such as the K9 glass can be described. The advantages of coupling the image analysis to images acquired by interferometry compared to conventional interferometric analysis are fast generation of large data amounts, low statistical uncertainty and independent measure of striae dimension and intensity.

This work demonstrates that most glasses can be ranked with respect to their striations by a very simple setup. Although striations are found and used in the ranking of the homogeneity of the glasses, it is likely that striations below the detection limit of the scanner exist in the investigated glasses. In other words, the glasses contain more striations than those detected by the scanner. These undetected striations are very weak striations similar to those that are believed to be present in the K9 glass. As these striations are very weak, the effect of such striations on the integral intensity is neglectable for most glasses. Therefore, the omission of the weak striations does not affect the stria characterisation of non-optical glasses.

### 4.3 The chemical origin of the striae

Although the image analysis method is proven to be a fast and reliable method for characterisation of striae in glasses, it fails to identify the chemical background of the striae. Since chemical striations can have several origins, a complete description of the chemical origin of all striae in a glass requires focus on several species

and their redox state. Hence, a full description of the chemical nature of all the glasses used in paper 3 is impossible and therefore, the study is limited to glasses obtained from the stone wool melts. As described in subsection 2.2.3, stone wool melts can contain both variations in both the chemical composition and in the oxidation state of iron. Since local fluctuations in chemical composition of various glasses have been described by techniques such as electron microprobe in earlier studies (see subsection 2.3.2), focus is in this work devoted to the description of local changes of the redox state of iron as quantification of local redox state is an almost unexplored research area.

Commonly, the oxidation state of iron in iron-bearing glasses is determined by means of Mössbauer spectroscopy [Fudali et al 1987; Bingham et al 1999; Kukudapu et al 2003; Bouhifd et al 2004; Jayasuriya et al 2004] or optical absorption spectroscopy [Kumar & Lin 1991; Ehrt et al 2001; Yamashita et al 2008]. Mössbauer spectroscopy is used for the characterisation of the average redox state of a glass, as a powder is employed for the analysis, i.e., the average oxidation state of the sample is obtained. In addition, the ferric iron content must account for at least 3 % of the total iron content to be measurable. In optical absorption spectroscopy, areas can be selected for measurements, but due to the spot size of the incident light, the resolution normally lies around 0.5 to 2 mm. Furthermore, if the glasses in addition to changes in redox composition possess local changes in the chemical composition, the extinction coefficient is not uniform across the glass. The presence of extinction coefficient variations causes errors in the determination of the iron redox state in the glass. Therefore, optical absorption spectroscopy is not considered suitable for quantitative determination of the iron oxidation state in glasses from stone wool melts.

The binding energy of iron in glass depends on its redox state [Mekki et al 1996]. Due to the higher charge of ferric iron, the interacting coulomb forces are stronger than those of ferrous iron and consequently ferric iron has a higher binding energy. Therefore, measurement of the binding energy of iron in glasses should be a feasible approach for the discrimination between ferrous and ferric iron. However, the binding energy of the 2p electron of  $\text{Fe}^{2+}$  in pure ferrous oxide and  $\text{Fe}^{3+}$  in pure ferric iron oxide is 709.2 and 711.2 eV, respectively [Brundle et al 1977]. Due to this small difference in binding energy and the fact that the binding energy of iron in glass depends on the chemical composition of the glass [Mekki et al 1996], the applicability of binding energy measurements in iron redox state determination must be further explored.

The binding energy of the iron ions in the glass is measured by means of X-ray photoelectron spectroscopy (XPS). Measurements with this highly surface sensitive method can be performed on selected areas of the sample. Due to the high surface sensitivity of the measurement only the upper ~20 nm of the sample are measured, i.e., only the surface area and not the bulk beneath the surface area is measured. Since the measured area is determined by the operator and only the upper ~20 nm of the sample are measured, it is possible to find a striated area on the sample and exclusively measure the redox state of iron in this area. Therefore, the technique might be valuable for the characterisation of the redox induced striae in glasses from stone wool melts. Despite its potential, XPS has only been applied in a few studies to determine the redox state of polyvalent elements in glass and mainly in simple glasses systems with few components [Yu et al 1997; Mekki & Salim 1999; Khattak et al 2004]. In order to strengthen the validity of the determination of the iron redox state in glasses from stone wool melts, the reliability of the XPS technique is initially explored by measuring the redox state of iron in well homogenised basalt glasses.

#### 4.3.1 Method verification

To produce homogeneous basalt glasses with varying iron oxidation state, a stem glass is produced from a basalt rock melted under reducing conditions. Due to the reducing conditions, a large fraction of the iron

oxide in the basalt rock is reduced to metallic iron that precipitates from the glass melt. Consequently the  $\text{Fe}_2\text{O}_3$  content in the stem glass is 2.4 wt% whereas that of the basalt rock is 9.7 wt%. The iron reduction provides the possibility to investigate the reliability of the method on glasses with low iron content. To produce a series of glasses with the same chemical composition, but varying iron redox ratio, the stem glass is melted in  $\text{Al}_2\text{O}_3$  crucibles in air at different temperatures. The melting temperature is a parameter for adjustment of the iron oxidation state since the reduced state becomes more stable at higher temperatures [Dingwell & Brearley 1988; Lange & Carmichael 1989; Magnien et al 2008]. The XPS Fe high resolution spectra of basalt glass produced at 1210 and 1500 °C are shown in Figure 4.11.

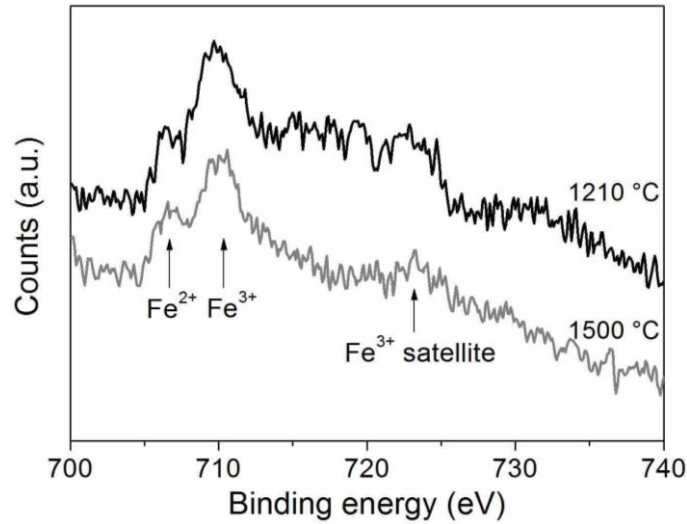


**Figure 4.11:** XPS Fe high resolution spectra of two basalt glasses produced in  $\text{Al}_2\text{O}_3$  crucible in air at 1210 and 1500 °C. The satellite at 723 eV is ascribed to the presence of  $\text{Fe}^{3+}$  [Brundle et al 1977].

At a binding energy of ~710 eV, two overlapping peaks are found. From the binding energy, the two peaks are ascribed to  $\text{Fe}^{2+}$  and  $\text{Fe}^{3+}$ . To determine the iron redox ratio, the area of each of the peaks must be determined as the atomic ratio between ferrous iron and ferric iron ( $\text{Fe}^{2+}/\text{Fe}^{3+}$ ) is equal to the peak area ratio of the two components in the XPS spectrum. The area of the ferrous and ferric iron peak is determined by deconvolution of the peak into the two subpeaks representing  $\text{Fe}^{2+}$  and  $\text{Fe}^{3+}$ . The content of ferric iron in the stem glass and the samples produced at various temperatures in  $\text{Al}_2\text{O}_3$  crucible in air is given in Table 4.3.

**Table 4.3:** The molar percentage of  $\text{Fe}^{3+}$  of the glasses prepared at different temperatures and in different crucibles. The standard deviation of the measurements is given.

	1210 $\text{Al}_2\text{O}_3$	1300 $\text{Al}_2\text{O}_3$	1400 $\text{Al}_2\text{O}_3$	1500 $\text{Al}_2\text{O}_3$	1600 $\text{Al}_2\text{O}_3$	Stem glass
$\text{Fe}^{3+}$ content	87.0±1.5 %	83.2±3.0 %	81.8±1.9 %	77.3±1.8 %	73.1±1.8 %	0 %

The content of ferric iron increases with decreasing temperature as expected due to an entropy effect (paper 4). The determined iron oxidation states are in agreement with those found by means of Mössbauer spectroscopy on other iron-bearing glass systems (paper 4). Therefore, it is inferred that XPS is a suitable method for the determination of the iron oxidation state in glasses.

### 4.3.2 Characterisation of glasses from stone wool melts

Mössbauer spectroscopy measurements on stone wool melts show that  $\text{Fe}^{3+}$  constitutes less than 3 % of the total iron content [Kirkegaard et al 2005; Lund et al 2010]. Despite this fact, small domains of the melt might contain ferric iron in concentrations above 3 %. To explore whether some of the striae in the glass from the

stone wool melt are caused by the presence of ferric iron, a sample from both the cupola and electric furnace is investigated (Figure 4.12).

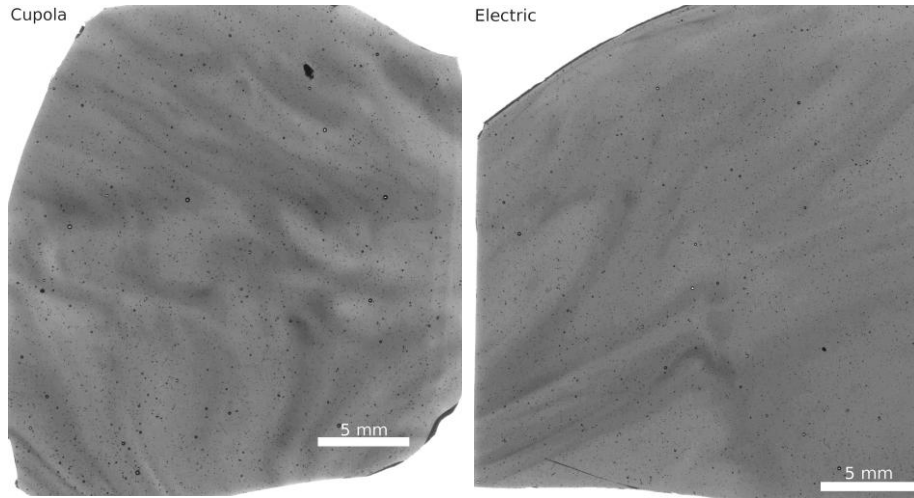


**Figure 4.12:** The glasses produced from stone wool melt in cupola and electric furnace. The samples are used for XPS investigation of potential domains containing  $\text{Fe}^{3+}$ . The brightness of the images has been optimised for printing.

Both the sample from the cupola and the electric furnace contain intense striae and these intensely striated areas are subjected to XPS measurement. The intensely striated areas are chosen as the presence of  $\text{Fe}^{3+}$  at the expense of  $\text{Fe}^{2+}$  strongly affects the optical light absorption of the glass and thereby the optical transmission of the glass, i.e., redox induced striations appear intense on transmission images. The samples are sputtered with argon plasma prior to the measurement to remove dust on the surface as dust leads to a lower signal to noise ratio. The subsequent measurement is performed with a spot size of  $400\ \mu\text{m}$ , which allows selection of a striated region without including the glass matrix in the analysis.

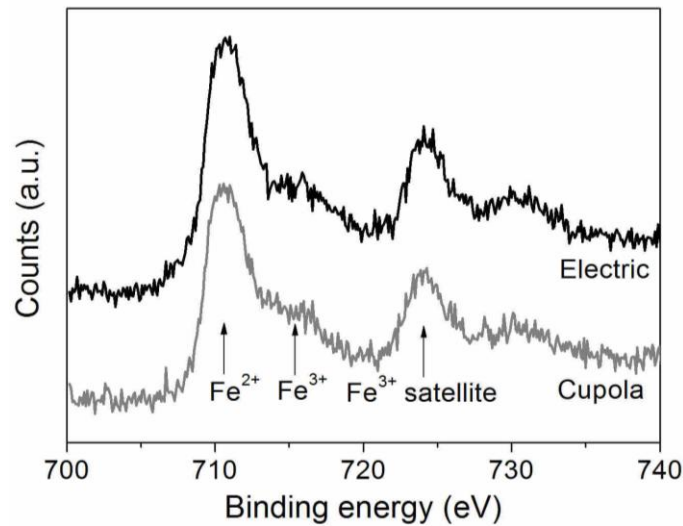


**Figure 4.13:** XPS Fe high resolution measurement of an intensely striated region in glass sampled from the cupola and electric furnace. The peak at  $724\ \text{eV}$  is a satellite associated to the presence of  $\text{Fe}^{3+}$  [Brundle et al 1977].

The XPS spectra of the glass from the cupola and electric furnace exhibit a large peak around  $711\ \text{eV}$  with a shoulder at higher binding energies. The peak is ascribed to  $\text{Fe}^{2+}$ , whereas the shoulder is believed to arise from the presence  $\text{Fe}^{3+}$ . The iron binding energies in the stone wool melt sample are higher than those in basalt, which is ascribed to the compositional influence on binding energy of iron. Since the iron concentration in the cupola and electric furnace is 2.5 and 3 times higher, respectively than that of the basalt glasses used for the measurements presented in Figure 4.11, the signal to noise ratio is better in the measurements

presented in Figure 4.13. The shoulder ascribed to  $\text{Fe}^{3+}$  is remarkable since Mössbauer spectroscopy measurements are unable to prove the presence of ferric iron, i.e., the ferric iron constitute less than 3 % of the total iron content. Upon deconvolution of the peak into subpeaks from ferrous and ferric iron, the content of  $\text{Fe}^{3+}$  in the measured area is 30 and 26 % of the total iron content for the sample from the electric and cupola furnace, respectively. Due to the detection of ferric iron, it is inferred that at least some of the intense striations in glasses shown in Figure 4.12 are caused by changes in the redox ratio of iron. As a consequence, the presence of  $\sim 25\%$   $\text{Fe}^{3+}$  is sufficient to create a sharp transmission gradient to the surrounding non-ferric iron containing glass matrix. The lack of a ferric iron sextet in Mössbauer spectroscopy spectra of glass from stone wool melts can appear counterintuitive, but this can be explained by two facts. First, in the investigated samples, the area measured by XPS constitutes about 0.02 % of the total sample area. Since only a very small part of the sample is measured, it is feasible that the ferric iron content in the entire sample is less than 3 % of the total iron content. Second, on purpose an intensely striated area is selected for the XPS measurement, i.e., it is unlikely that domains with significantly higher ferric iron content are present in the glass.

From the XPS measurements it can be inferred that the glass from stone wool melt produced in cupola and electric furnaces contains striae with a minor fraction of  $\text{Fe}^{3+}$ . In contrast iron is solely present in its ferrous state in the glass matrix. These local changes in iron oxidation state can either reflect the existence of local redox conditions inside the melting furnace or their creation can have taken place after the melt has left the furnace, i.e., oxygen in the atmosphere has oxidised the reduced glass melt during the sampling procedure. In addition to the redox induced striae, the presence of striae caused by changes in the chemical composition is considered likely. The investigation of such striae requires XPS high resolution spectra of several species at several spots on and around a stria. Furthermore, as each stria can possess a different chemical nature, the measurement procedure has to be performed on several striae to clarify the chemical origin of the striae in a certain glass type.

## 4.4 Bubble characterisation

To determine the bubble content in glass sampled from a stone wool melt produced in a cupola furnace, the glass is initially ground and polished to a thickness where the glass becomes optically transparent. The glass contains visible bubbles and smaller bubbles that require the use of a microscope to be detected. Since the large bubbles are scarce, but affect the total bubble volume fraction of the glass to a large extent, these bubbles are excluded from a statistical bubble analysis. To investigate the bubbles in the volume of the glass, stacks of images are acquired according to the arguments presented in section 2.5. Each stack has a depth of 90  $\mu\text{m}$  and as an image is acquired for each 3  $\mu\text{m}$ , the stack consists of 30 2D images. To improve the statistical accuracy of the bubbles analysis, 4 image stacks are acquired of each sample (paper 5).

### 4.4.1 Bubble size distribution

Due to the rare occurrence of large bubbles and their large impact on the bubble volume, only bubbles with a volume between 1.8 and 40  $\mu\text{m}^3$  are included in the statistical bubble analysis. Identified objects with a size below 1.8  $\mu\text{m}^3$  mainly arise from noise and are therefore excluded from the analysis. With respect to the number of bubbles, the bubbles in the range 1.8 to 40  $\mu\text{m}^3$  constitute at least 99.9 %. The number of bubbles at a given volume fraction is presented in Figure 4.14. The number of bubbles is an average of the 4 analysed stacks, where the dimension of each stack is 230x230x90  $\mu\text{m}^3$  ( $4.76 \cdot 10^6 \mu\text{m}^3$ ).

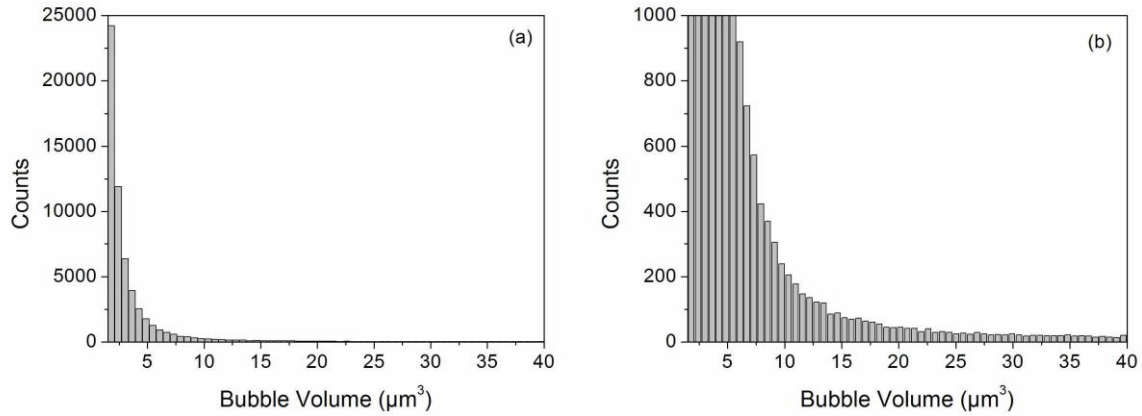


**Figure 4.14:** The average number of bubbles in an image stack as a function of the bubble volume. (a) The entire region of interest, i.e., bubble volumes from 1.8 to 40  $\mu\text{m}^3$  (b) magnification on the ordinate.

Although a glass volume of just  $4.76 \cdot 10^{-3} \text{ mm}^3$  is inspected, 60,000 bubbles are identified. The number of bubbles at a given volume fraction increases drastically with decreasing bubble size. Although the number of bubbles appears profuse, the total volume of the bubbles with a volume of 1.8 to 40  $\mu\text{m}^3$  is  $1.63 \cdot 10^5 \mu\text{m}^3$ , i.e., 3.4 vol% of the glass. The total bubble volume fraction is larger than 3.4 % since bubbles with a volume larger than 40  $\mu\text{m}^3$  are excluded from the analysis.

Automatic bubble counting by means of the object counter 3D plugin on image stacks can easily and swiftly identify very large number of bubbles and is therefore considered to be a useful approach for exploring how the bubble content is influenced, e.g., by the melting temperature and the chemical composition of the melt.

#### 4.4.2 Chemical analysis of gaseous species

Although analysis of image stacks is a powerful tool for the evaluation of the bubble size distribution, the chemical species inside the bubbles remain unrevealed. To shed light on the chemical nature of the bubbles, vacuum hot extraction is performed. During the vacuum hot extraction, the sample is placed in a chamber at vacuum and the gasses released from the sample during heating are measured by means of a mass spectrometer. The specific measurement procedure is described in paper 5. As mentioned, the glass from the stone wool melt contains both bubbles visible to the naked eye and bubbles that require the use of microscope to be observed. Since different gasses might be present in the small and large bubbles, vacuum hot extraction is performed on both the bulk glass and a glass powder with a diameter smaller than 25  $\mu\text{m}$ . Several gasses are found in the glass. In the powder sample, the carbon containing species  $\text{CH}_4$ ,  $\text{CO}$  and  $\text{CO}_2$  are dominating, i.e., these gasses are present in the small bubbles as discussed in paper 5. Analysis of the bulk sample and subsequent comparison of this with the analysis of the powder sample identifies that the large bubbles contain  $\text{N}_2$ ,  $\text{SO}_2$  and  $\text{H}_2\text{S}$ . Quantification of the content of the gaseous species is carried out by determination of the integrated ion current for a given mass to charge ratio ( $m/z$ ). Since the mass of the molecules  $\text{CO}$  and  $\text{N}_2$  is identical, the content of each of the gasses cannot be determined, instead the sum of the content of the two gasses is given (Figure 4.15).

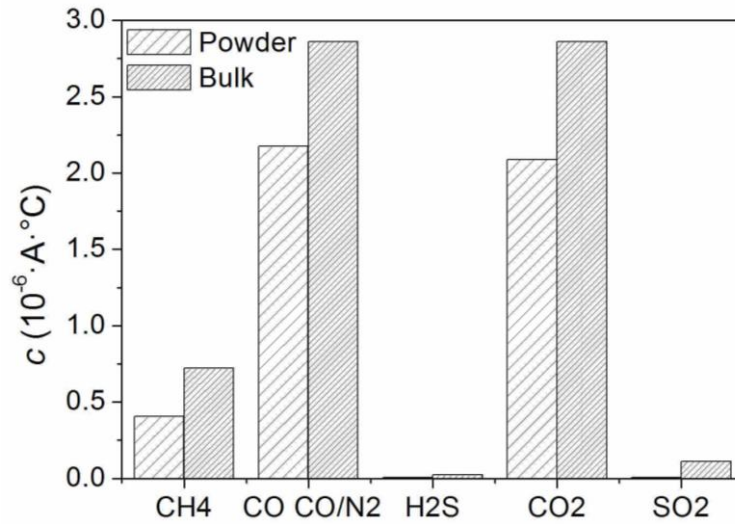


**Figure 4.15:** The integrated ion current of the mass spectroscopy signal ( $c$ ) for the powder and the bulk sample. In the bulk sample, both  $N_2$  and  $CO$  are present, and hence the mass spectroscopy signal at  $m/z = 28$  covers both  $N_2$  and  $CO$ . The carbon containing species are the dominating gases in the bubbles. The content of species such as  $CH_4$  and  $CO_2$ , which are found in the small bubbles is larger in the bulk sample. This finding is a result of the milling process since some of the small bubbles have been opened during the milling and consequently, a part of the gas has been released during the sample preparation. Therefore, the increased content of  $CH_4$  and  $CO_2$  in the bulk sample compared to the powder sample does not imply that these two gases are found in larger bubbles. The sulphur containing gasses in the large bubbles are created from sulphur impurities in the raw materials, whereas  $CH_4$ ,  $CO$  and  $CO_2$  are believed to arise from the combustion of coke and reaction between coke and iron oxides as discussed in paper 5. The hydrogen source for  $CH_4$  and  $H_2S$  is considered to be moisture in the raw materials.

## 5 Influence of production conditions on inhomogeneities

### 5.1 Equilibration of striae in glass melts

When describing the elimination of chemical striae, discrimination between striae caused by changes in chemical composition and redox state is necessary. Differences in the chemical composition create an entropy driven driving force for the equilibration of the chemical differences according to the second law of thermodynamics. Since the equilibration occurs by means of diffusion, the diffusion length ( $x$ ) and the stria size ( $D$ ) determine whether a stria is eliminated during the melting process. An equilibration reduces both the size of the stria and the chemical difference between the stria and the surrounding melt whereas elimination refers to complete removal of the stria from the melt. The diffusion length of the  $i$ 'th component in the melt is determined by Eq. (5.1):

$$x_i = k_i \cdot t^{1/2} \quad (5.1)$$

Where  $t$  is the diffusion time and  $k$  is a component specific constant, which depends on the viscosity of the melt. A stria is a three dimensional domain in the glass, but for any 2D cross section of the striae, there is a line where the stria has its largest dimension as illustrated in Figure 5.1.

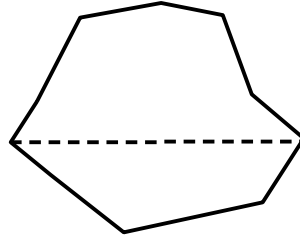


**Figure 5.1:** Cross section of a striated domain. The dotted line shows the largest dimension of the striae in the cross section.

Since diffusion occurs from the entire interface between the striated domain and the surrounding homogeneous glass melt, complete elimination of the stria occurs when the diffusion length is equal to or larger than half of the largest striae dimension, as expressed by Eq. (5.2)

$$x \geq \frac{1}{2} \cdot D \quad (5.2)$$

When  $x < \frac{1}{2} \cdot D$ , the diffusion length is insufficient to eliminate the entire striated region, but equilibration of the stria occurs. Therefore when  $x < \frac{1}{2} \cdot D$ , the size of the striated domain shrinks, but a part of the stria persists in the melt.

#### 5.1.1 Effect of stirring on striae in glass melts: Simulation studies

To elucidate the effect of stirring on the striations in a glass melt, the simulated ideal striae from subsection 4.1.1 is initially considered due to its simplicity. By means of image processing, the ideal striation is subjected to one or two times stirring of  $360^\circ$  (Figure 5.2) as elaborated in paper 6.

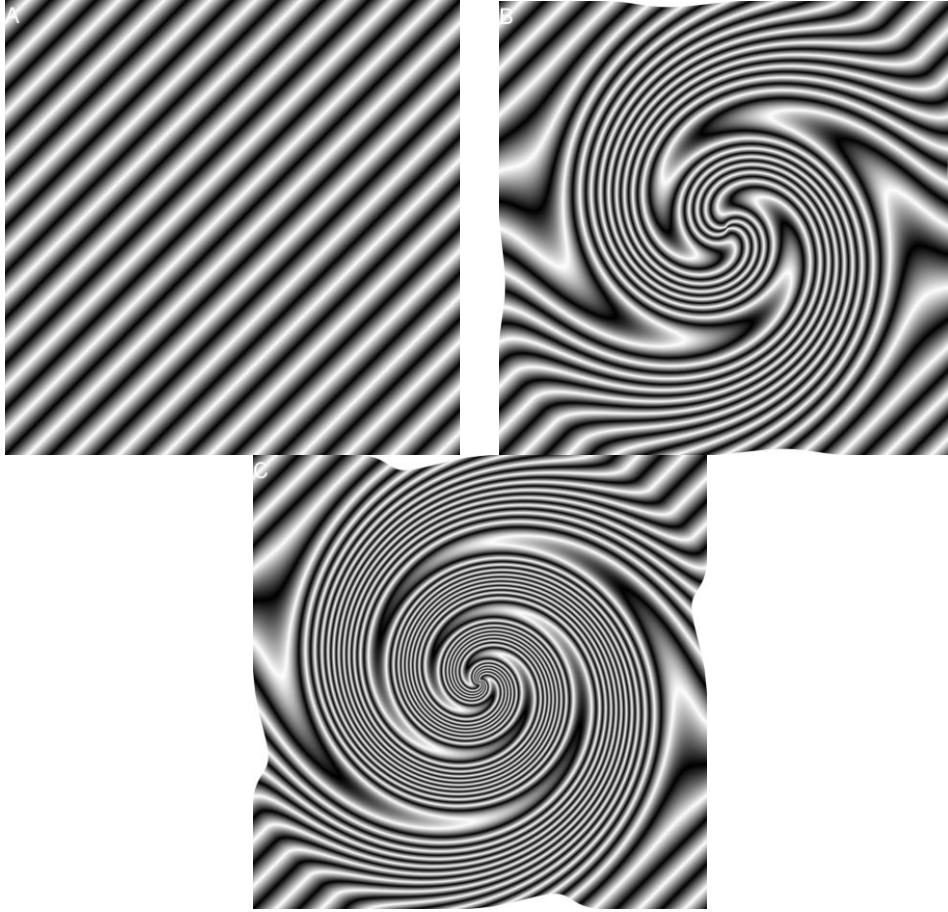


**Figure 5.2:** Images of an ideal stria with a striae size of 200 pixels (A) and the same ideal stria subjected to one (B) and two times (C) of 360° stirring.

Stirring exerts the striae in the melt to shear forces that deform the striae. At the corners of the image, the stria structure remains intact despite the stirring. The same phenomenon is observed in real glass furnaces where “dead zones” exist, i.e., simultaneous to a laminar flow in the majority of the glass furnace volume, unaffected dead zones are present in the furnace. The dead zones are commonly found in the corners of melting furnaces, which is an observation similar to the one seen in the simulation in Figure 5.2. The effect of stirring on the ideal striation is found by Fourier transformation of line scans on the images (Figure 5.3).

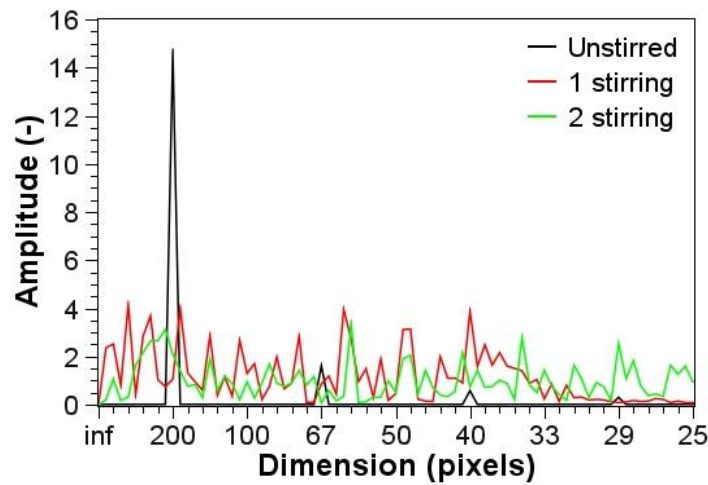


**Figure 5.3:** Fourier transformation spectra of ideal striation (Unstirred) and the same stria subjected to a simulated 360 ° stirring for 1 time (1 stirring) or 2 times (2 stirring).

As the chemical differences leading to striae only can be equilibrated through diffusion of the species that are in excess or depleted in the striation, the area under the curves in the Fourier transformation spectra is identical. In other words, the integral intensity of the stria is unaffected by the stirring. Whereas the ideal striation exhibits a well-defined peak at a striae dimension of 200 pixels and minor peaks due to model artefacts (discussed in subsection 4.1.1), the Fourier transformation spectra of the stirred striations have numerous peaks. The presence of numerous peaks in the Fourier transformation spectrum of the stirred striation reflects the creation of a broad range of stria sizes during stirring. In other words, stirring distributes the dimensions of the initial striae to a broad range of dimensions, i.e., both smaller and larger striae are created during stirring. The overall stria intensity is, however, unaffected by the stirring process. Conversion of the large 200 pixel striae to striae with a size smaller than 30 pixels requires two times stirring of 360 °. The difference in the content of striae smaller than 30 pixels between the striation subjected to one and two times 360 ° stirring reflects the requirement of a certain extent of the stirring to inflict the conversion of large striae to smaller ones.

Since the diffusion process occurs at the interface between the stria and the glass matrix, small striae are eliminated faster than the larger ones. Stirring of glass melts increases the homogenisation rate as it distributes the initial stria size to smaller and larger dimensions. The redistribution of the striae size distribution to smaller striae ensures that a larger percentage of the striae fulfil the elimination criterion in Eq. (5.2). After equilibration of the small striae, a subsequent stirring deforms the large remaining striae and creates new small striae. In a continuously stirred glass melt, the small striae are eliminated by diffusion and the remaining larger striae continuously undergo conversion to small striae. Therefore, in a glass melt that contains both small and large striae, stirring is an efficient approach to increase the homogenisation rate. To verify the theoretical considerations, simple stirring experiments are performed.

### 5.1.2 Effect of stirring on striae in glass melts: Experiments

The effect of stirring on the stria equilibrate rate is examined for a borosilicate melt since it is convenient to handle as the melt can be homogenised at 1120 °C and since the melt has a very good glass forming ability. To produce well-defined and easily detectable striations, a glass from the same borosilicate melt doped with 0.4 wt% CoO is produced as described in detail in paper 6. The striations are introduced by synthesising a clear, homogeneous borosilicate melt followed by addition of 0.75 g of the CoO doped glass to the clear melt. After the addition of the blue CoO doped glass, the melt is subjected to various stirring durations up to 15 min. The stirring creates a laminar flow in the glass [Cable 1996], which can convert large striae to smaller ones.

On the scanned images of the samples, one pixel has an area of  $7.9 \times 7.9 \mu\text{m}^2$ . As any change in optical transmission requires at least two pixels, structures with a size above  $16 \mu\text{m}$  can be detected. During the integration of Fourier transformation spectra, the integration proceeds from large to small dimensions. Therefore, the integral intensity at  $20 \mu\text{m}$  is a measure of the total stria content ( $I_{20}$ ) in the glass. The total stria content ( $I_{20}$ ) against stirring duration is shown in Figure 5.4. The melt is subjected to a melting period of 15 min, i.e., for stirring durations shorter than 15 min, the remaining time is retention (paper 6).

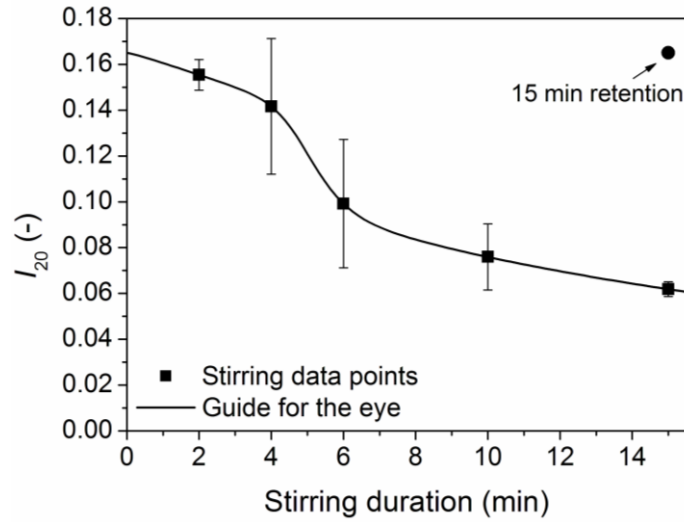


**Figure 5.4:** Total stria content ( $I_{20}$ ) against stirring duration. As the total melting period is 15 min, melts subjected to less than 15 min stirring have a retention period subsequent to the stirring. The total stria content in an unstirred melt is added for comparison. The errors bars are calculated from the three samples prepared from each melt.

The stria content decreases with increasing stirring duration in an inversely s-shaped manner. Comparison of the melt subjected to stirring during the entire 15 min melting period and the melt solely subjected to retention reveals a decrease in the stria content of 63 % in the stirred melt. As a decrease in stria content is obtained without altering the melt temperature and the melting duration, the diffusion length  $x$  in Eq. (5.1) is identical for all melts. Initially, the size of the striae is 1-2 mm as this is the size of the CoO doped glass pieces added to the melt. During stirring, shear forces convert the large striae to smaller ones. Therefore, in the stirred melt, a larger fraction of the striae fulfils the criterion in Eq. (5.2) compared to the unstirred melt. For stirring durations shorter than 4 min, the impact of stirring on the stria content is limited as the striae content in melts exposed to stirring durations shorter than 4 min is similar to the stria content in the unstirred melt. From the limited effect, it is inferred that optimum conversion of striae requires at least 4 min. A similar phenomenon is observed during the simulation as 2 rounds of stirring are required to obtain a full conversion of the striae. Hence, a certain degree of stirring is required to obtain stria size conversion. The critical stria conversion time can be reduced by optimisation of the stirrer geometry [Cable 1986]. Further decrease in stria content for stirring durations longer than 4 min is ascribed to a combination of stria conversion and diffusion. The small striae created as a result of the stirring in the beginning of the stirring period are eliminated within the melting period of 15 min. After equilibration of the small striae, the stirring ensures that the remaining large striae are converted to new small striae that can be equilibrated within the time frame of the experiment. In other words, the conversion of large striae into smaller ones is a continuous process that takes place during stirring of a striated glass melt.

### 5.1.3 Effect of melting temperature and retention time on stria equilibration

In some industrial furnaces, establishment of stirring facilities is costly and in reducing furnaces such as cupola furnaces, the use of stirrers is complicated. The reducing conditions in the cupola prevent the use of platinum stirrers as platinum alloys it is when exposed to reducing conditions. The application of brittle ceramic stirrers is impeded by the addition of raw material as lumps that mechanically can damage the stirrer. To reveal other approaches than stirring for improvement of the stria equilibration rate, the impact of melt temperature and retention time on stria equilibration rate is investigated for stone wool melts.

To replicate the conditions in a cupola furnace, melting experiments are performed in a 7 L SiC-clay crucible doped with graphite to expose the melt to reducing conditions. The large volume of the melting crucible enables the utilisation of raw materials used in stone wool production. The batch denoted SW1 is produced from two basalts and a briquette containing basalt, bauxite, dolomite, hematite and stone wool waste embedded in a cement matrix. The experimental details and the chemical composition of the raw materials and the batch are provided in paper 7.

Melts produced at 1300 °C for 10 and 20 min contain large amounts of undissolved white stones. To identify the origin of the undissolved material, the stones are separated from the glass phase and subjected to chemical analysis. 51.9 mol % CaO and 44.3 mol % MgO in the stones identify that the undissolved material is dolomite. As dolomite is the last dissolving component in the glass melt, striae enriched in CaO and MgO are expected to occur around the undissolved stones. The redox conditions of the melt are monitored by determination of the iron redox state in the melt. To study the redox conditions, a sample from the longest retention time (40 min) is investigated as the sample exerted to the longest retention time is the sample closest to thermodynamic equilibrium. The Mössbauer spectrum of the sample melted at 1300 °C for 40 min is shown in Figure 5.5.

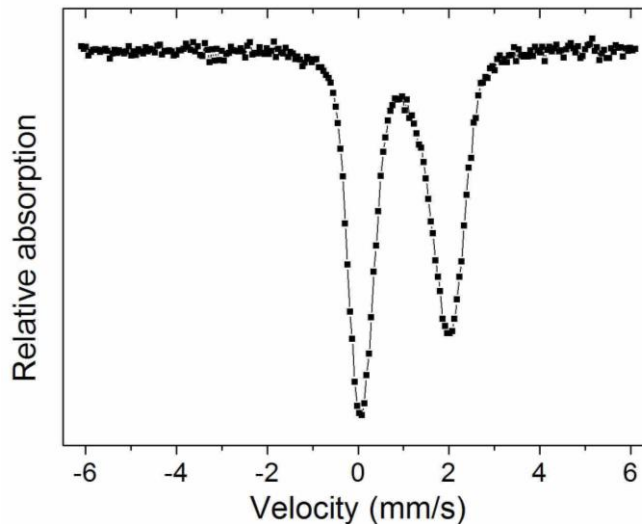


**Figure 5.5:** Mössbauer spectroscopy spectrum of sample melted at 1300 °C for 40 min. The duplet in the spectrum is caused by the presence of  $\text{Fe}^{2+}$  in the glass.

The presence of a single duplet in the Mössbauer spectroscopy spectrum (Figure 5.5) reveals the presence of  $\text{Fe}^{2+}$  in the glass network. As the spectrum exhibits no signs of a  $\text{Fe}^{3+}$  sextet, the  $\text{Fe}^{3+}$  content is below the detection limit of 3 % of the total iron content, i.e., ferrous iron constitute at least 97 % of the total iron content in the glass network. The lack of ferric iron in the glass structure agrees with the formation of a metallic iron pool at the bottom of the crucible during the melting process. The reduced state of iron in the glass melt is similar to that found in stone wool melts produced in cupola furnaces [Kirkegaard et al 2005; Lund et al 2010]. As the iron oxidation state shifts to more reduced conditions upon increasing melt temperature [Lange & Carmichael 1989; Kukkadapu et al 2003; Magnien et al 2008; Borisov & McCammon 2010], iron is believed to be in its ferrous state in the glasses produced at temperatures higher than 1300 °C.

The total stria content ( $I_{20}$ ) in glasses produced at melt temperatures from 1300 to 1450 °C with retention times of 10 to 40 min is shown in Figure 5.6.

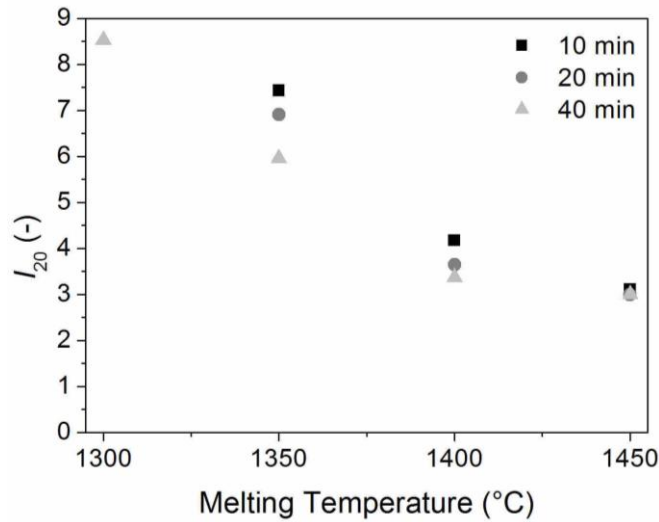


**Figure 5.6:** Total stria content ( $I_{20}$ ) as a function of melting temperature for retention times of 10, 20 or 40 min. Due to the presence of undissolved raw material, it has not been feasible to prepare a samples for stria characterisation for retention times of 10 and 20 min at 1300 °C.

The stria content in the glasses reduces upon either increase in the melt temperature or prolonging of the retention time. The impact of the melt temperature on glass homogeneity decreases at melting temperatures above 1400 °C as the decrease in  $I_{20}$  for samples prepared at 1400 and 1450 °C is small. At higher melt temperature, the impact of increased retention time on the stria equilibration diminishes. Both phenomena can be explained by different chemical natures of the striae. As the glass melt contains several different species originating from a spectrum of raw materials, striae enriched/depleted in different species are believed to exist in the melt. The ions in the melt differ in parameters such as charge and ionic radius and consequently, each ion has a given mobility in the melt. The more mobile ions exhibit a larger diffusion length for fixed melting conditions than the less mobile ones. At a low melt temperature such as 1350 °C, the elimination of stria caused by mobile ions requires a time frame of at least 40 min. Therefore, a gradual equilibration of the striae (gradual reduction of  $I_{20}$ ) occurs up to a retention time of 40 min at 1350 °C. At higher melting temperatures such as 1450 °C, elimination of striae enriched/depleted in mobile ions proceeds within about 10 min. Consequently, for retention times longer than 10 min, mainly striae enriched/depleted in ions with low mobility exist in the melt, which decreases the stria equilibration rate. The lower stria equilibration rate is reflected by a small effect of retention time on  $I_{20}$  at 1450 °C. Similarly, for a temperature increase from 1400 to 1450 °C at a given retention time, the majority of the chemical differences caused by the mobile ions can be eliminated at a temperature of 1400 °C. After the fast equilibration of striae caused by mobile ions, the gradients in slowly diffusing species remain in the melt and therefore the homogeneity improvement rate is controlled by the diffusion of these slowly diffusing species. In summary, at low melting temperatures and retention times, a fast improvement of the homogeneity is observed, whereas at higher melting temperatures and longer retention times, the stria equilibration is controlled by slowly diffusion species, and this slows the homogenisation process. The difference of the diffusion rate of various ions in calcium containing silicate melts has been verified in earlier studies [Van Orman et al 2001; MacKenzie & Canil 2008]. The diffusion rate of various species can vary by as much as two orders of magnitude in soda-lime-silica glass melt [Rüssel 1991].

A second stone wool melt (SW2) is investigated and the batch composition of SW2 is similar to that of SW 1. The SW2 batch is made solely from briquettes containing wool waste, diabase, anorthosite, olivine, and slag embedded in a cement matrix. After 20 min at 1400 °C, the SW2 glass contains undissolved stones,

i.e., melts produced from the SW2 batch are clearly more inhomogeneous than melts produced from the SW1 batch. Hence, the homogeneity of a glass melt depends on the raw materials in the batch. Due to the large prevalence of undissolved material in the SW2 glass, it has not been possible to prepare a sample for stria characterisation. From XRF measurement, the chemical composition of the undissolved stones is found to be (wt %): 48.9 SiO<sub>2</sub>, 29.6 Al<sub>2</sub>O<sub>3</sub>, 15.3 CaO and 2.9 Na<sub>2</sub>O. The undissolved stones are identified as anorthosite as the chemical composition anorthosite in the batch is (wt %): 48.5 SiO<sub>2</sub>, 29.0 Al<sub>2</sub>O<sub>3</sub>, 13.8 CaO and 2.9 Na<sub>2</sub>O.

#### 5.1.4 Effect of melt viscosity on stria equilibration

According to the Stoke-Einstein equation, the diffusion rate in a liquid medium is inversely proportional to the viscosity of the medium. To explore the influence of viscosity on stria equilibration, the SW1 batch is melted under more oxidising conditions at 1400 °C. The redox state of the melt is altered by coating the surface of the crucible with a Cr<sub>2</sub>O<sub>3</sub> refractory paste. The paste prevents contact between the melt and the graphite in the crucible, which removes the reducing power of the graphite from the glass melt. As polyvalent element, iron is particularly sensitive to changes in redox state and glass produced in the Cr<sub>2</sub>O<sub>3</sub> crucible is expected to contain both ferrous and ferric iron in the glass structure. However, due to the more oxidising conditions, the metallic iron formation is reduced when the crucible is coated with the Cr<sub>2</sub>O<sub>3</sub> paste. Therefore, the iron oxide concentration in the melt produced in Cr<sub>2</sub>O<sub>3</sub> coated crucible is higher than in the melt produced in the as-obtained SiC crucible. In the SiC crucible, iron is present as Fe<sup>2+</sup>, i.e., metallic iron formation removes network modifier from the melt, which should increase the melt viscosity [Mysen & Richet 2005]. In the Cr<sub>2</sub>O<sub>3</sub> coated crucible, the melt has higher iron oxide content, but XPS measurement (see paper 4) on melt produced in the Cr<sub>2</sub>O<sub>3</sub> coated crucible reveals that 60 % of the iron is present as Fe<sup>3+</sup> (network former) whereas the remaining 40 % are Fe<sup>2+</sup> (network modifier). The larger iron oxide content in the melt produced in the Cr<sub>2</sub>O<sub>3</sub> crucible should decrease the viscosity if iron acts as a network modifier, but the presence of Fe<sup>3+</sup> increases the melt viscosity since Fe<sup>3+</sup> is a network former in the melt. Therefore, in addition to the difference in the structural role of iron between melts produced in the two crucibles, the chemical composition of the melts differs. The impact of each of the two effects on the melt viscosity is difficult to quantify from theoretical considerations. During casting of the melts, it is from visual observation clear that the melt produced in the Cr<sub>2</sub>O<sub>3</sub> coated crucible has a higher viscosity than the melt produced in the as-obtained SiC crucible. The increase in melt viscosity due to the application of the Cr<sub>2</sub>O<sub>3</sub> paste is therefore ascribed to the conversion of Fe<sup>2+</sup> to Fe<sup>3+</sup>.

As the homogenisation process is expected to be slower in the Cr<sub>2</sub>O<sub>3</sub> coated crucible than in the SiC crucible due to the higher viscosity of the melt, a melt temperature of 1350 °C is expected to be insufficient to produce melts that after 10 min retention possess a homogeneity that fulfils the requirement for grinding and polishing. However, since increasing melt temperature shifts the iron oxidation state towards the reduced state, high melt temperatures vanish the effect of the Cr<sub>2</sub>O<sub>3</sub> paste. Through this trade-off, the total stria content in glass produced in the two crucibles is compared for a melt temperature of 1400 °C (Figure 5.7).

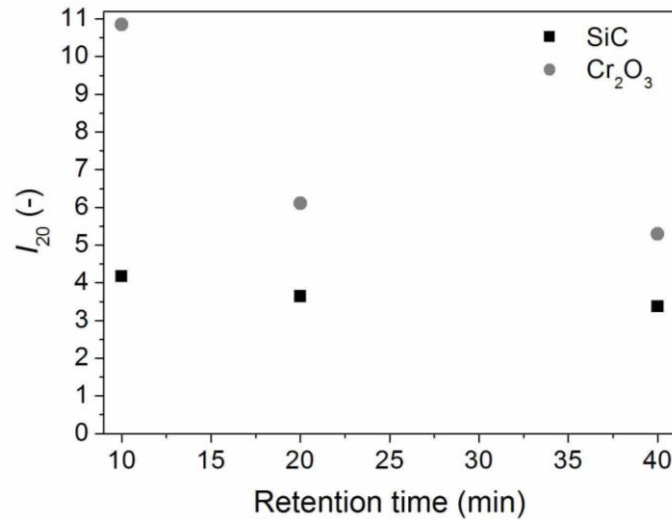


**Figure 5.7:** Total stria content ( $I_{20}$ ) in melts produced in crucible coated with  $\text{Cr}_2\text{O}_3$  refractory paste ( $\text{Cr}_2\text{O}_3$ ) and as-obtained crucible (SiC) at 1400 °C.

The total stria content is higher in glasses prepared in the  $\text{Cr}_2\text{O}_3$  coated crucible than in glass produced in the as-obtained crucible. The  $\text{Cr}_2\text{O}_3$  refractory paste can dissolve into the glass melt, which is investigated by measurement of the  $\text{Cr}_2\text{O}_3$  content in the glasses. For retention times of 10, 20 and 40 min, the  $\text{Cr}_2\text{O}_3$  content in the glass is 0.11, 0.19 and 0.86 wt%, respectively. The largest homogeneity difference between glasses produced in the two crucible types occurs for retention times of 10 and 20 min, i.e., the glasses with the lowest  $\text{Cr}_2\text{O}_3$  content. Therefore, it is inferred that the homogeneity difference between glasses produced in the two crucibles originates from other factors than  $\text{Cr}_2\text{O}_3$  enriched striae. A large  $\text{Cr}_2\text{O}_3$  content in the melt is not equivalent to many or intense striations as no striations are created by homogeneously distributed large  $\text{Cr}_2\text{O}_3$  content. However, as  $\text{Cr}_2\text{O}_3$  dissolves into the melt at the interface between the melt and the  $\text{Cr}_2\text{O}_3$  paste, a homogeneous distribution of  $\text{Cr}_2\text{O}_3$  in the melt is considered infeasible at the applied retention times.

The increased stria content in the viscous melts produced in the  $\text{Cr}_2\text{O}_3$  coated crucible demonstrates that the viscosity indeed influences the stria equilibration rate in the melt. The difference in stria content between glasses produced in the two crucibles types diminishes when the retention time is prolonged. This trend can be explained by the same phenomenon responsible for the decreasing effect of increasing retention time on stria content at higher melt temperatures (cf. subsection 5.1.3). Finally, the viscous melt is by visual inspection found to contain more bubbles with a size above ~2 mm than melts produced in the as-obtained SiC crucible. Hence, besides impeding ionic movement required for stria equilibration, the increased viscosity reduces the ascent rate of the bubbles.

## 5.2 Removal of bubbles from glass melts

If the retention time is sufficiently long at an appropriately elevated temperature, the glass melt is bubble free as buoyancy provides a driving force for the bubbles to ascend to the surface and escape the melt. However, since most industrially produced glasses are subjected to a limited retention time, bubbles can exist in glasses. To improve the bubble removal from the glass melt, scientists and technologists have through decades studied the effect of fining agents on bubble removal [Stelzner et al 1990; Beerkens et al 2007; Grund et al 2009]. Fining agents release gasses during the melting process that cause the formation of larger bubbles

through coalescence of small bubbles. The formation of larger bubbles enhances the ascent rate of the bubbles in the glass melt.

In this work, the influence of other parameters on the bubble content in stone wool melts is explored. In detail, the influence of melting temperature and iron content of the melt is investigated for stone wool melts produced in cupola furnaces.

### 5.2.1 Influence of melt temperature on bubble content

The bubble size distribution in glasses from stone wool melts with the same chemical composition sampled from the same cupola furnace at the same day at 1455 and 1485 °C is studied (Figure 5.8). The normal operating temperature of the furnace is 1455 °C and a temperature increase has been obtained by slightly increasing the coke content in the batch. The experimental procedure of the study is described in detail in paper 5.

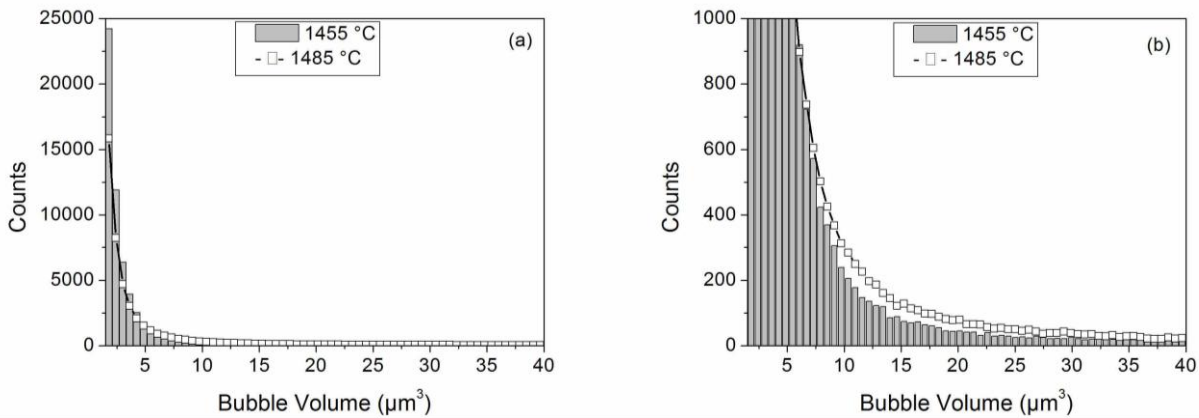


**Figure 5.8:** The average number of bubbles in an image stack as a function of the bubble volume. The counting has been conducted on rapidly cooled melts produced at 1455 and 1485 °C, respectively. (a) The entire region of interest, i.e., bubble volumes from 1.8 to 40  $\mu\text{m}^3$  (b) magnification on the ordinate.

From the glasses produced at 1455 and 1485 °C, it is observed that the number of small bubbles (2-6  $\mu\text{m}^3$ ) is larger in the former melt than in the latter one (Figure 5.8a). The difference in bubble number between the samples becomes increasingly pronounced with decreasing bubble volume. Concerning the larger bubbles (> 7  $\mu\text{m}^3$ ), the reverse effect is seen, i.e., the number of larger bubbles increases with melting temperature (Figure 5.8b). To quantify the change in the bubble size distribution, the 84 % threshold, i.e., the diameter below which 84 % of the bubbles are found, is calculated. The 84 % threshold increases from 5.66 to 8.13  $\mu\text{m}$  when the temperature is increased from 1455 to 1485 °C (Table 5.1), which reflects a growth of the bubbles when the temperature is elevated from 1455 °C to 1485 °C.

**Table 5.1:** The total volume of bubbles in the range 1.8-40  $\mu\text{m}^3$  in the stone wool melts prepared at 1455 and 1485 °C. The 84 % bubble diameter threshold based on the number of bubbles is also given.

Temperature	84 % Threshold	Volume ( $\mu\text{m}^3$ )
1455 °C	5.66 $\mu\text{m}$	163320
1485 °C	8.13 $\mu\text{m}$	168600

Besides affecting the bubble size distribution, the temperature increase can alter the gas solubility in the melt. The gas solubility influences the total volume of bubbles in the glass melt since a large solubility enables dissolution of small bubbles in the glass structure. To explore whether the temperature difference affects the gas solubility in the melt to a measurable extent, the volume of the bubbles in the size range 1.8-40  $\mu\text{m}^3$  is calculated (Table 5.1). The difference in the bubble volume between the two melts is within the statistical uncertainty and therefore the total bubble volume is concluded to be similar in the two melts. This implies

that the temperature increase from 1455 to 1485 °C only creates another bubble size distribution since the overall bubble volume in the glass is similar for both melt temperatures. Hence, a temperature change of 30 °C is insufficient to inflict any detectable change in gas solubility based on the investigation of bubbles with a volume of 1.8-40  $\mu\text{m}^3$ . Since the gas solubility in the glass structure depends on the temperature of the melt, it is believed that a large temperature difference would have caused a detectable difference in the bubble volume. The growth of the bubbles due to the temperature elevation from 1455 °C to 1485 °C can take place through coalescence of small bubbles leading to the formation of larger ones. Hence, the number of small bubbles diminishes, but since the former small bubbles are part of larger bubbles, the overall volume remains constant. The thermodynamic driving force for the coalescence is a decrease of the surface energy as the volume to surface ratio increases when the bubble size increases. However, the coalescence can be hindered kinetically by a high viscosity of the melt. As the viscosity decreases with increasing temperature, the kinetic barrier for formation of large bubbles is easier to overcome at 1485 °C than at 1455 °C. Therefore, the temperature increase promotes the coalescence rate. Despite a growth of the bubbles, the ascent rate remains below the rate required to ascent to the top of the melt and to escape the melt.

### 5.2.2 Influence of iron on bubble content

The bubble content in an iron-bearing stone wool melt and a low iron-bearing stone wool melt is compared (Figure 5.9). The chemical composition of the two melts is comparable except for the FeO content which is around 1 wt% in the low iron-bearing stone wool melt and 6 wt% in the traditional iron-bearing stone wool melt.

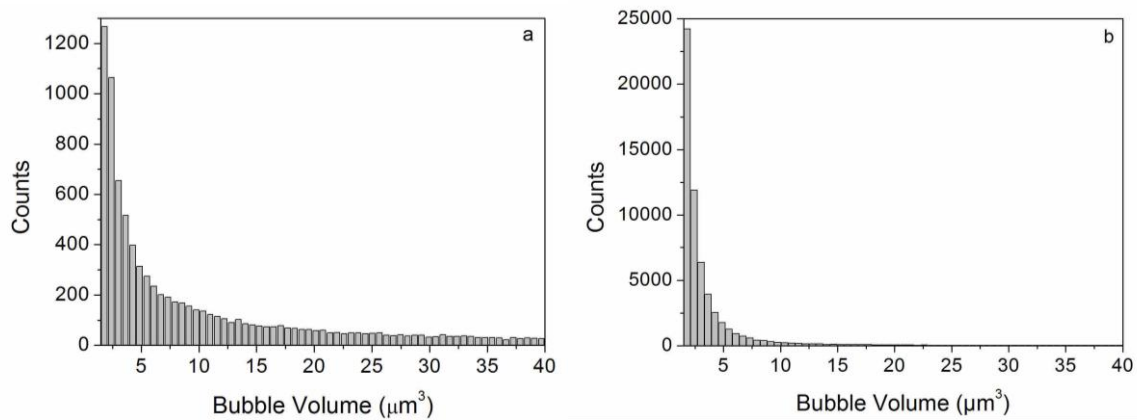


**Figure 5.9:** The average number of bubbles in an image stack with a volume of 230x230x90  $\mu\text{m}^3$  for melts produced in a cupola furnace. (a) Low iron-bearing stone wool melt with a FeO content around 1 wt%. (b) Traditional iron-bearing stone wool melt with 6 wt% FeO.

The number of small bubbles is more than one order of magnitude smaller in the low iron-bearing melt than in the iron-bearing stone wool melt. Despite the large difference in the number of bubbles, the total bubble volume based on bubbles in the range 1.8 to 40  $\mu\text{m}^3$  is 78598  $\mu\text{m}^3$  in the low iron iron-bearing melt compared to 163320  $\mu\text{m}^3$  in the iron-bearing melt. Hence, whereas the number of bubbles is an order of magnitude higher in the low iron-bearing melt compared to the traditional iron-bearing stone wool melt, the bubble volume only differs by a factor of two between the two melts. The bubble volume is less dependent on the iron concentration than the number of bubbles since mainly the amount of small bubble differs between the two melts. From Figure 4.15 it is known that the small bubbles mainly contain the carbon containing species  $\text{CH}_4$ ,  $\text{CO}$  and  $\text{CO}_2$ . As the amount of small bubbles is dramatically lower in the low iron-bearing stone wool melt, it is inferred that the creation of small bubbles is linked to the presence of iron ions in the melt. Iron

oxide can undergo redox reaction with coke to produce metallic iron and CO/CO<sub>2</sub>. The ratio of CO to CO<sub>2</sub> depends on the redox conditions inside the furnace. Furthermore, CO can react with C and H<sub>2</sub>O to CH<sub>4</sub> if moisture and reducing conditions are present at high temperature. Since formation of metallic iron is observed in the furnace, it is believed that the generation of small bubbles with carbon containing gaseous species originates from the reaction between iron oxide and coke.

## 6 Summary

In this work, a novel stria characterisation method based on optical transmission of light is developed. A fast data acquisition rate is obtained by analysing a grey image of the investigated glass. The grey image consists of a set of dots (pixels) each with a grey value that by calibration is converted to an optical transmission. In other words, the image contains millions of small squares that each reflects the optical transmission of the glass at that spot. The optical transmission changes in the glass are quantified by performing line scans. During line scanning, the transmission is recorded along a line inserted on the image. For each sample 500 line scans are performed and the line scans are subsequently subjected to Fourier transformation. From the Fourier transformation spectrum, the stria intensity at a given stria dimension is determined. The stria intensity is a measure of the sum of the transmission difference between the striae and the glass matrix at a certain stria dimension. The total stria content of the glass is found by integration of the stria intensity. Besides determination of the total stria content in a glass, a characteristic intensity and dimension are determined from the plot of the integral intensity against stria dimension.

In addition to striae, inhomogeneous glasses contain bubbles of varying size. On images, the bubbles appear with a transmission difference to the surrounding glass. Since the stria characterisation method detects transmission differences on the image, bubbles are detected as intense striae. To omit the impact of bubbles on the stria characterisation, the bubbles are prior to line scanning removed from the image by image processing.

In this work, a scanner is applied for the image acquisition. The detection limit of the scanner allows stria characterisation of non-optical glasses. To extend the application of the stria characterisation method to optical glasses, improvement of the image acquisition technique to optical microscopes or interferometers is required. By employing a scanner as image acquisition technique, non-optical glasses can be ranked with respect to their stria content. The stria characterisation method developed in this work has an improved detection limit compared to the commonly applied refractive index measurements.

Striae are removed from glass melts through diffusion of the species that are enriched or depleted in the striae. Complete elimination of a stria occurs when the diffusion length is larger than half the size of the stria. The elimination of striae from glass melts is explored by stirring and increase in melt temperature or retention time. During stirring of a glass melt, the dimension of the initial striae is broadened to both larger and smaller dimensions. The creation of smaller striae improves the stria equilibration rate as the elimination of small striae requires a smaller diffusion length than the elimination of large striae. In other words, stirring in itself does not eliminate striae, but stirring improves the stria equilibration rate by converting larger striae to smaller ones. Both increasing melt temperature and prolonged retention time enhance the melt homogeneity with respect to striae. At increasing melt temperature, the effect of retention time on the stria content of the melt diminishes, which is ascribed to the presence of striae with different chemical origins. At high melt temperature, striae enriched/depleted in quickly diffusing species are equilibrated after a short retention time and consequently for prolonged retention times the equilibration of the remaining striae is controlled by slowly diffusing species. Hence, for glass melts with striae of different chemical origin, the effect of retention time on the stria content reduces when the melt temperature is increased. An increase in the melt viscosity at a constant melt temperature reduces the stria equilibration rate.

The chemical origin of striae in stone wool melts is addressed by X-ray photoelectron spectroscopy (XPS). Although the content of  $\text{Fe}^{3+}$  by Mössbauer spectroscopy is known to be below the detection limit of 3

%, small domains with up to 25 %  $\text{Fe}^{3+}$  are identified by means of XPS. Therefore, some of the striae in the iron bearing glasses from stone wool melts are caused by the presence of a minor part of  $\text{Fe}^{3+}$ .

Besides striae, some glasses contain bubbles. The bubbles size distribution and bubble volume in glasses are assessed by acquiring 2D image stacks of the sample. An image stack contains a set of optical transmission images of a given area inspected at different depths. Size determination of the bubbles proceeds through identification of the core of the bubble in the image stack followed by determination of the bubble diameter.

An increase of the melt temperature from 1455 to 1485 °C of a stone wool melt produced in a cupola furnace affects the bubbles size distribution in the melt. The melt temperature increase shifts the bubble size distribution towards larger bubbles although the total bubble volume is unaffected by the temperature increase. Bubbles with a size below 25  $\mu\text{m}$  are filled with the carbon containing species  $\text{CH}_4$ ,  $\text{CO}$  and  $\text{CO}_2$ . Larger bubbles mainly contain  $\text{N}_2$ ,  $\text{H}_2\text{S}$  and  $\text{SO}_2$ .

The presence of carbon containing species suggests the reduction of iron oxide by coke as a potential bubble formation source. To verify this, a melt containing 6 wt%  $\text{FeO}$  and a similar melt with 1 wt%  $\text{FeO}$  are produced in a cupola furnace. The number of small bubbles known to contain the carbon containing species reduces by more than one order of magnitude when reducing the  $\text{FeO}$  content from 6 to 1 wt%. This strongly indicates that the generation of carbon containing gaseous inclusions originates from the reaction between iron oxide and coke.

## 7 Bibliography

- Abramoff M. D., Magelhaes P. J. & Ram S. J. (2004) Image processing with ImageJ. *Biophoton. Int.*, **11**, 36-42.
- Abrams M. B. & Green D. J. (2006) Prediction of crack propagation and fracture in residually stressed glass as a function of the stress profile and flaw size distribution. *J. Eur. Ceram. Soc.*, **26**, 2677-2684.
- Afghan M. & Cable M. (1980) Estimation of the homogeneity of glass by the Christiansen filter method. *J. Non-Cryst. Solids*, **38/39**, 3-8.
- Aylward N. H., Cable M. & Wang S. S. (1986) Some practical problems in estimating the homogeneity of glass by the Christiansen filter method. *Indian Ceram. Soc.*, **2**, 281-287.
- Backnaes L., Stelling J., Behrens H., Goettlicher J., Mangold S., Verheijen O., Beerkens R. G. C. & Deubener J. (2008) Dissolution mechanisms of tetravalent sulphur in silicate melts: evidences from sulphur K-edge XANES studies on glasses. *J. Am. Ceram. Soc.*, **91**, 721-727.
- Balasubramanian K., Jacobson M. R. & Macleod H. A. (1992) New Christiansen filters. *Appl. Opt.*, **31**, 1574-1587.
- Beerkens R. G. C. & van der Schaaf J. (2006) Gas release and foam formation during melting and fining of glass. *J. Am. Ceram. Soc.*, **89**, 24-35.
- Beerkens R. G. C. (2007) Sulphur chemistry and sulphur fining and foaming of glass melts. *Glass Technol.: Eur. J. Glass Sci. Technol. A*, **48**, 41-52.
- Behrens H. & Haack M. (2007) Cation diffusion in soda-lime-silicate glass melts. *J. Non-Cryst. Solids*, **353**, 4743-4752.
- Bingham P. A., Parker J. M., Searle T., Williams J. M. & Fyles K. (1999) Redox and clustering of iron in silicate glasses. *J. Non-Cryst. Solids*, **253**, 203-209.
- Bolte S. & Cordelières F. P. (2006) A guided tour into subcellular colocalization analysis in light spectroscopy. *J. Microsc.*, **224**, 213-232.
- Borisov, A. & McCammon, C. (2010) The effect of silica on ferric/ferrous ratio in silicate melts: An experimental study using Mössbauer spectroscopy. *Am. Mineral.*, **95**, 545-555.
- Bouhifd M. A., Richet P., Besson P., Roskosz M. & Ingrin J. (2004) Redox state, microstructure and viscosity of a partially crystallized basalt melt. *Earth Planet. Sci. Lett.*, **218**, 31-44.
- Braetsch V. & Frischat G. H. (1988) Shelyubskii method of studying phase separation in the system  $\text{Li}_2\text{O}-\text{SiO}_2$ . *J. Am. Ceram. Soc.*, **71**, C376-377.
- Brundle C. R., Chuang T. J. & Wandelt K. (1977) Core and valence level photoemission studies of iron oxide surfaces and the oxidation of iron. *Surf. Sci.*, **68**, 459-468.
- Brückner R. (1980) *Schlieren (Glas in Glas)*. In *Glastechnische Fabrikationsfehler* by H. Jebsen-Marwedel & R. Brückner. Springer Verlag, Berlin, Germany.
- Cable M. (1986) Quantitative model studies of stirrers for laboratory glass melts. *J. Non-Cryst. Solids*, **80**, 642-648.
- Cable M. (1996) Model studies of the homogenizing of laboratory glass melts. *J. Non-Cryst. Solids*, **196**, 309-313.
- Canil D. (1999) Vanadium partitioning between orthopyroxene, spinel and silicate melt and the redox states of mantle source regions for primary magmas. *Geochim. Cosmochim. Acta*, **63**, 557-572.
- Chopin M.-H., Gouillart E., Papin S. & Toplis M. J. (2010) Influence of limestone grain size on glass homogeneity. *Glass Technol.: Eur. J. Glass Sci. Technol. A*, **51**, 116-122.
- Christiansen C. (1884) Untersuchungen über die optischen Eigenschaften fein verteilter Körper, erste Mitteilung. *Ann. der Phys.*, **23**, 298-306.
- Christiansen C. (1885) Untersuchungen über die optischen Eigenschaften fein verteilter Körper. Zweite Mitteilung. *Ann. Der Phys.*, **24**, 439-446.

- Davis K. M., Agarwal A., Tomozawa M. & Hirao K. (1996) Quantitative infrared spectroscopic measurement of hydroxyl concentrations in silica glass. *J. Non-Cryst. Solids*, **203**, 27-36.
- De Freitas J. M. & Player M. A. (1995) Ultrahigh precision measurements of optical heterogeneity of high quality fused silica. *Appl. Phys. Lett.*, **66**, 3552-3554.
- Dingwell D. B. & Brearley M. (1988) Melt densities in the CaO-FeO-Fe<sub>2</sub>O<sub>3</sub>-SiO<sub>2</sub> system and the compositional dependence of the partial molar volume of ferric iron in silicate melts. *Geochim. Cosmochim. Acta*, **52**, 2815-2825.
- Ehrt D., Leister M. & Matthai A. (2001) Polyvalent elements iron, tin and titanium in silicate, phosphate and fluoride glasses and melts. *Phys. Chem. Glasses*, **42**, 231-239.
- Fudali R. F., Darby Dyar M., Griscom D. L. & Schreiber H. D. (1987) The oxidation state of iron in tektite glass. *Geochim. Cosmochim. Acta*, **51**, 2749-2756.
- Grofmeier M., Natrup F. V. & Bracht H. (2007) Barium diffusion in mixed cation glasses. *Phys. Chem. Chem. Phys.*, **9**, 5822-5827.
- Grund L., Jonson B. & Lundstedt K. (2009) The influence of basicity on oxygen activity and antimony oxide fining efficiency in alkali alkaline earth aluminosilicate glasses. *Glass Technol.: Eur. J. Glass Sci. Technol. A*, **50**, 241-246.
- Hoffmann H.-J. (1999) Does Shelyubskii's evaluation method characterize the homogeneity of glass? *Glasstech. Ber. Glass. Sci. Technol.*, **72**, 99-102.
- Hoffmann H.-J. (2000) Theory of the spectral transmittance of Christiansen filters made of glass beads. *Appl. Phys. B*, **70**, 853-861.
- Hoffmann H.-J. (2003) Theory of spectral transmittance of Christiansen filters. *Glass Sci. Technol.*, **76**, 285-297.
- Huang X. L., Xu Y. G., Lo C. H., Wang R. C. & Lin C. Y. (2007) Exsolution lamellae in a clinopyroxene megacryst aggregate from Cenozoic basalt, Leizhou peninsula, South China. *Contrib. Mineral. Petrol.*, **154**, 691-705.
- Inoue S., Yamane M. & Serizawa T. (1984) An apparatus for precise measurement of glass homogeneity by Shelyubskii's method. *Ceram. Bull.*, **63**, 1412-1415.
- Janke A. & Frischat G. H. (1998) Improved homogeneity of various glasses by gas film levitation. *Glastech. Ber. Glass Sci. Technol.*, **71**, 193-198.
- Jayasuriya K. D., O'Neill H. St. C., Berry A. J. & Campbell S. J. (2004) A Mössbauer study of the oxidation state of Fe in silicate melts. *Am. Mineral.*, **89**, 1597-1609.
- Jerie K., Pawlik E. M., Wójcik J. & Bieganski P. (1999) Determination of non-homogeneity in vitreous glasses by means of positron annihilation and analysis of electron microscope images. *J. Non-Cryst. Solids*, **258**, 155-160.
- Kaufmann J. & Rüsel C. (2010) Thermodynamics of the Cu<sup>+</sup>/Cu<sup>2+</sup>-redox equilibrium in aluminosilicate melts. *J. Non-Cryst. Solids*, **356**, 1615-1619.
- Kerkhof F. (1980) *Optische Verfahren zur Erfassung von Schlieren*. In *Glastechnische Fabrikationsfehler*. by H. Jebben-Marwedel & R. Brückner. Springer Verlag, Berlin, Germany.
- Khattak G. D., Mekki A., Wenger L. E. (2004) Local structure and redox state of copper in tellurite glasses. *J. Non-Cryst. Solids*, **337**, 174-181.
- Kirkegaard, L. F., Korsgaard, M. & Yue, Y. Z. (2005) Redox behavior of iron bearing glass fibers during heat treatment under atmospheric conditions. *Glass. Sci. Technol.*, **78**, 1-6.
- Kreyszig E. (1999). *Advanced Engineering Mathematics*. John Wiley & Sons, Singapore. ISBN: 0-471-33328-X.
- Kukkudapu R. K., Li H., Smith G. L., Crum J. D., Jeoung J.-S., Poisl W. H. & Weinberg M. C. (2003) Mössbauer and optical spectroscopic study of temperature and redox effects on iron local environments in a Fe-doped (0.5 mol% Fe<sub>2</sub>O<sub>3</sub>) 18Na<sub>2</sub>O-72SiO<sub>2</sub> glass. *J. Non-Cryst. Solids*, **317**, 301-318.
- Kumar B. & Lin S (1991) Redox state of iron and its related effects in the CaO-P<sub>2</sub>O<sub>5</sub>-Fe<sub>2</sub>O<sub>3</sub> glasses. *J. Am. Ceram. Soc.*, **74**, 226-228.
- Lange R. A. & Carmichael I. S. E. (1989) Ferric-Ferrous equilibria in Na<sub>2</sub>O-FeO-Fe<sub>2</sub>O<sub>3</sub>-SiO<sub>2</sub> melts: Effects of analytical techniques on derived partial molar volumes. *Geochim. Cosmochim. Acta*, **53**, 2195-2204.

- LaTourette T., Hervig R. L. & Holloway, J. R. (1995). Trace element partitioning between amphibole, phlogopite, and basanite melt. *Earth Planet. Sci. Lett.*, **315**, 13-30.
- Leth-Miller R., Jensen A. D., Glarborg P., Jensen L. M., Hansen P. B. & Jørgensen S. B. (2003). Investigation of a mineral melting cupola furnace. Part I. Experimental work. *Ind. Eng. Chem. Res.*, **42**, 6872-6879.
- Lund, M. D. & Yue, Y. Z. (2008). Fractography and tensile strength of glass wool fibres. *J. Jap. Ceram. Soc.*, **116**, 841-845.
- Lund, M. D. Yue, Y. Z. & Lybye, D. (2010) Impact of the oxidation state of iron on the tensile strength of stone wool fibres. *Glass Technol.: Eur. J. Glass Sci. Technol. A*, **51**, 97-102.
- MacKenzie J. M. & Canil D. (2008) Volatile heavy metal mobility in silicate liquids: Implication for volcanic degassing and eruption prediction. *Earth Planet. Sci. Lett.*, **269**, 488-496.
- Magnien V., Neuville D. R., Cormier L., Roux J., Hazemann J.-L., De Ligny D., Pascarelli S., Vickridge I., Pinet O. & Richet P. (2008) Kinetics and mechanisms of iron redox reactions in silicate melts: The effects of temperature and alkali cations. *Geochim. Cosmochim. Acta*, **72**, 5157-5168.
- Mekki A., Holland D., McConville C. F., Salim M. (1996) An XPS study of iron sodium silicate glass surfaces. *J. Non-Cryst. Solids*, **208**, 267-276.
- Mekki A. & Salim M. (1999) XPS study of transition metal doped silicate glasses. *J. Electron. Spectrosc. Relat. Phenom.*, **101-103**, 227-232.
- Mulfinger H. O. (1980) *Gase (Blasen) in der Glasschmelze*. by H. Jebsen-Marwedel & R. Brückner. Springer Verlag, Berlin, Germany.
- Mysen, B. & Pichet, P. (2005) *Silicate glasses and melts. Properties and structure*. Elsevier, Amsterdam, The Netherlands, ISBN: 0444520112.
- Nehring F., Jacob D. E., Barth M. G & Foley S. F. (2008) Laser-ablation ICP-MS analysis of siliceous rock glasses fused on an iridium strip heater using MgO dilution. *Microchim. Acta*, **160**, 153-163.
- Persson H. R. (1983) *Glass Technology Manufacturing & Properties*. Cheong Moon Gak Publishing Co., Seoul, Korea.
- Pertermann M. & Hirschmann M. M. (2003) Partial melting experiments on a MORB-like pyroxenite between 2 and 3 GPa: Constraints on the presence of pyroxenite in basalt source regions from solidus location and melting rate. *J. Geophys. Res.*, **108**, ECV 12-1-12-7.
- Puryayev D. T. (1998) Interferometric method to measure and test the optical homogeneity of transparent materials. *Opt. Laser Technol.*, **30**, 235-238.
- Raman C. V. (1949) The theory of the Christiansen experiment. *Proc. Indian Acad. Sci.*, **29**, 381-390.
- Rocholl A. (1999) Major and trace element composition and homogeneity of microbeam reference material: Basalt glass USGS BCR-2G. *J. Geostand. Geoanal.*, **22**, 33-45.
- Rüssel C. (1991) Self diffusion of polyvalent ions in a soda-lime-silica glass melt. *J. Non-Cryst. Solids*, **134**, 169-175.
- Schilling G. & Weiss W. (1966) Experiments to determine the homogeneity of glasses by Shelyubskii method. *Glass Technol.*, **7**, 66-71.
- Schmidt M. W., Dardon A., Chazot G. & Vannucci R. (2004) The dependence of Nb and Ta rutile-melt partitioning on the melt composition and Nb/Ta fractioning during subduction process. *Earth Planet. Sci. Lett.*, **226**, 415-432.
- Schoo U. & Mehrer H. (2000) Diffusion of <sup>22</sup>Na in sodium borate glasses. *Solid State Ionics*, **130**, 243-258.
- Širok B., Blagojević B. & Bullen P. (2008) *Mineral Wool*. Woodhead Publishing Limited, Cambridge, England. ISBN: 978-1-4200-7045-3.
- Shelby J. E. (2005) *Introduction to glass science and technology*. The Royal Society of Chemistry, Cambridge, England. ISBN: 0-85404-639-9.
- Shelyubskii V. I. (1960) A new method for determining and controlling glass uniformity. *Glass Ceram.*, **17**, 412-418.

- Smedskjaer M. M., Mauro J. C., Sen S., Deubener J. & Yue Y. Z. (2010) Impact of network topology on cationic diffusion and hardness of borate glass surfaces. *J. Chem. Phys.*, **133**, 154509.
- Souza L. A., Leite M. L. G., Zanotto E. D. & Prado M. O. (2005) Crystallization kinetics. A new tool to evaluate glass homogeneity. *J. Non-Cryst. Solids*, **351**, 3579-3586.
- Stelzner T., Heide K. & Kothe K. (1990) Extraction of oxygen during heat-treatment of silicate melts under vacuum conditions. *Glass Technol.*, **31**, 236-239.
- Stolper E. (1982) Water in silicate glasses: an infrared spectroscopic study. *Contrib. Mineral. Petrol.*, **81**, 1-17.
- Svecova B., Spirkova J., Nekvidova P., Mika M. & Svecova L. (2010) Ion exchange as a new tool to evaluate and quantify glass homogeneity. *J. Non-Cryst. Solids*, **356**, 1509-1513.
- Sylvester P. (2006) Trends in analytical development and earth science applications in LA-ICP-MS and LA-MC-ICP-MS for 2004 and 2005. *Geostand. Geoanalyt. Res.*, **30**, 197-207.
- Tenzler T. & Frischat G. H. (1995) Application of the Christiansen-Shelyubskii method to determine homogeneity and the refractive index of industrial glasses. *Glastech. Ber. Glass Sci. Technol.*, **68**, 381-388.
- Tooley F. V. & Tiede R. L. (1946) Influence of batch mixing time and batch grain size on homogeneity of a soda-lime-silica glass. *J. Am. Ceram. Soc.*, **29**, 197-199.
- Trejos T. & Almirall J. R. (2005) Sampling strategies for the analysis of glass fragments by LA-ICP-MS Part I. Micro-homogeneity study of glass and its application to the interpretation of forensic evidence. *Talanta*, **67**, 388-395.
- Van Orman J. A., Grove T. L. & Shimizu N. (2001) Rare earth element diffusion in diopside: influence of temperature, pressure, and ionic radius, and an elastic model for diffusion in silicates. *Contrib. Mineral. Petrol.*, **141**, 687-703.
- Varshneya A. K. (1986) Glass homogeneity measurement using Shelyubskii technique. *J. Non-Cryst. Solids*, **80**, 688-692.
- Varshneya A. K., Loo M. C. & Soules T. F. (1985) Glass inhomogeneity measurement using the Shelyubskii method. *J. Am. Ceram. Soc.*, **68**, 380-385.
- Vetere F., Behrens H., Misiti V., Ventura G., Holtz F., Rosa R. D. & Deubener J. (2007) The viscosity of shoshonitic melts (Vulcanello peninsula, Aeolian islands, Italy): Insight on the magma ascent in dikes. *Chem. Geol.*, **245**, 89-102.
- Villian O., Calas G., Galois L. & Cormier L. (2007) XANES determination of chromium oxidation states in glasses: comparison with optical absorption spectroscopy. *J. Am. Ceram. Soc.*, **90**, 3578-3581.
- Wilke M., Partzsch G. M., Bernhardt R., Lattard D. (2005) Determination of the iron oxidation state in basaltic glasses using XANES at the K-edge. *Chem. Geol.*, **220**, 143-161.
- Wondraczek L., Behrens H., Yue Y. Z., Deubener J. & Scherer G. W. (2007) Relaxation and glass transition in isostatically compressed diopside glass. *J. Am. Ceram. Soc.*, **90**, 1556-1561.
- Yamashita M., Akai T., Sawa R., Abe J. & Matsumura M. (2008) Effect of the preparation procedure on the redox states of iron in soda-lime silicate glass. *J. Non-Cryst. Solids*, **354**, 4534-4538.
- Yu X. Y., Day D. E., Long G. J. & Brow R. K. (1997) Properties and structure of sodium-iron phosphate glasses. *J. Non-Cryst. Solids*, **215**, 21-31.
- Yue Y. Z., von der Ohe R. & Jensen S. L. (2004) Fictive temperature, cooling rate and viscosity of glasses. *J. Chem. Phys.*, **120**, 8053-8059.
- Yue Y. Z. (2008) Characteristic temperatures of enthalpy relaxation in glass. *J. Non-Cryst. Solids*, **354**, 1112-1118.